Hindawi
Geofluids
Volume 2021, Article ID 7278131, 23 pages
https://doi.org/10.1155/2021/7278131

Review Article

Application of 3D Printing Technology in the Mechanical Testing of Complex Structural Rock Masses

Yingjie Xia,[1,2] Qingkun Meng,[1] Chuanqing Zhang,[2] Ning Liu,[3] Zhenxing Zhao,[4] Jun Chen,[3] and Gao Yang[2]

[1]*State Key Laboratory of Coastal and Offshore Engineering, Dalian University of Technology, Dalian 116024, China*
[2]*State Key Laboratory of Geomechanics and Geotechnical Engineering, Institute of Rock and Soil Mechanics, Chinese Academy of Sciences, Wuhan, Hubei 430071, China*
[3]*Power China Huadong Engineering Corporation, Hangzhou, Zhejiang 310014, China*
[4]*China Railway Construction Bridge Engineering Bureau Group 3rd Engineering Co., Shenyang, Liaoning 110043, China*

Correspondence should be addressed to Chuanqing Zhang; cqzhang@whrsm.ac.cn

Received 28 August 2021; Accepted 17 September 2021; Published 13 October 2021

Academic Editor: Yu Wang

In the engineering of underground construction, the discontinuous structures in rock mass have important influences on the mechanical behaviors of the subsurface of rock mass. The acquisition of mechanical parameters is the basis of rock mass engineering design, construction, safety, and stability evaluation. However, the mechanical parameters and failure characteristics of the same rock mass under different mechanical conditions cannot be obtained due to the limitations of specimen preparation techniques. In recent years, with the continuous development of 3D printing (3DP) technology, it has been successfully applied to the repetitive preparation of rock mass samples. The combinations of 3DP and other techniques, such as 3D scanning and CT scanning, provided a new approach to study the mechanical behavior of complex structural rock masses. In this study, through a comprehensive review of the technical progress, equipment situation, application fields, and challenges of the use of 3DP technology, the following conclusions were obtained: (1) 3DP technology has advantages over traditional rock mass specimen preparation techniques, and the verification of test results using 3D printed samples shows that the 3DP has broad application prospects in geotechnical engineering. (2) The combination of 3DP and other advanced techniques can be used to achieve the accurate reconstruction of complex structural rock masses and to obtain the mechanical and failure characteristics of the same rock mass structure under different mechanical boundary conditions. (3) The development of 3DP materials with high strength, high brittleness, and low ductility has become the major bottleneck in the application of 3DP in geotechnical engineering. (4) 3D printers need to meet the high precision and large size requirements while also having high strength and long-term printing ability. The development of 3D printers that can print different types of materials is also an important aspect of the application of 3DP in geotechnical engineering.

1. Introduction

Rock mass is characterized by discontinuity, inhomogeneity, and anisotropy. It is composed of various weak structural joints within certain engineering scales [1–4]. The internal structures of rock mass are generally complex and contain defects such as pores, joints, and fissures that directly affect the strength, deformation, and seepage characteristics of the rock mass, which are closely related to the stability of rock engineering [5–8]. Therefore, the mechanical behavior and failure characteristics of complex structural rock masses have become the key factors of rock mass engineering design, construction, safety, and stability evaluation [9–11].

Currently, the acquisition of mechanical parameters of rock mass is carried out using three main methods: in situ field tests [12–14], laboratory tests [15, 16], and numerical simulation [17, 18]. Specifically, in situ testing is the most effective method of obtaining the mechanical parameters of rock mass on an engineering scale. However, the large size of rock mass specimens used in in situ testing causes many

problems, such as a long test period, high costs, and influences on construction, leading to less data being obtained through in situ testing. Laboratory tests have been the most important means of obtaining the mechanical parameters of rocks because they can visualize the mechanical characteristics, such as the strength, deformation, and failure characteristics, of rock mass specimens under different mechanical boundary conditions. However, due to the limitations of the testing equipment in terms of the size of rock samples and the difficulty in preparing samples of complex structures, it is hard to obtain the mechanical parameters via laboratory tests. Moreover, since the experimental testing of rocks is generally destructive, it is impossible to accurately obtain the change rule of mechanical properties of the same rock mass. Numerical simulation has the advantages of low cost and repeatability, so it has become an effective supplement to in situ tests and laboratory tests on rock masses. However, the complex structures of rock mass are often simplified in the simulation process due to the limitations of calculation conditions, making the numerical model differ from the real structures of rock mass. In addition, the selection of material parameters and determination of constitutive relation in the simulation process would affect the calculation results [19–21].

As was discussed above, when laboratory tests are used to study the mechanical and failure properties of rock mass, the specimens need to be representative of their structural characteristics. Due to the complexity of natural rock mass structures, it is difficult to obtain rock mass specimens with identical structures and properties. So, it is impossible to obtain the mechanical properties of the same rock mass structure under different mechanical boundary conditions. Such problems can be solved by using similar material model tests. However, it is difficult to make specimens with natural joint surfaces, special internal structures, and chamber excavation models, although these structural characteristics have important influences on the strength, deformation, and failure characteristics of rock masses [22–25]. Therefore, the repetitive preparation of complex structural specimens is the key to carrying out laboratory tests.

As an additive manufacturing technology, the 3DP differs from traditional manufacturing techniques such as cutting and grinding because it uses a layer-by-layer accumulation method to achieve the precise reconfiguration of complex structures. In recent years, the 3DP has been widely used in many fields such as biomedicine, aerospace, automobile manufacturing, and electronic components [26–29]. With the development of 3DP technology, some studies have begun to explore the applications of 3DP in the field of rock mechanics. For example, the combination of technologies of 3DP, stress freezing technique, CT scanning, and X-ray scanning has enabled the quantitative characterization and visualization of complex structures inside deep rock masses [30–34]. Based on this technology, transparent natural sand conglomerate specimens have been produced to investigate the effects of complex structures on the stress field and plastic zone [35, 36]. Furthermore, some materials such as polylactic acid (PLA), gypsum, and photosensitive resin have also been used in the preparation of rock-like specimens. The feasibility of 3DP in rock mechanics tests was initially verified by comparing the mechanical and failure properties of rock specimens [37, 38]. After that, several regular rock masses were assessed using 3DP, and the influences of the structural characteristics on the overall mechanical properties were studied [39–41]. Recently, the 3DP technique has been applied to the structural reconstruction of irregular columnar jointed rock masses, and the feasibility and superiority of this method in the reconstruction of complex structural rock masses have been demonstrated by comparing the results of mechanical and laboratory tests [42–44].

Thus, it is clear that the 3DP has advantages over other techniques used in rock mechanics testing, such as the accurate and rapid specimen preparation of complex structural rock masses [45]. However, compared with the mechanical and failure characteristics of high strength and high brittleness in rock mechanics tests, the specimens prepared using 3DP usually have low strength and high plasticity, which limit the applications of 3DP in rock engineering. Therefore, on the basis of 3DP technology in complex structural rock mass reconstruction and mechanical testing, the applications and progress of the use of 3DP technology in the rock mass are reviewed from the aspects of materials, equipment, and test methods. In addition, the deficiencies of current 3DP technology in rock mass engineering are discussed to provide guidance for its engineering application.

2. The Technologies, Materials, and Equipment of 3DP

2.1. The Technologies of 3DP. The difference between 3DP technologies and traditional methods lies in the printing materials and accumulation methods. Table 1 describes the common 3DP technologies and their corresponding materials, which are mainly divided into three categories: (1) Extrusion 3DP technology includes fused deposition manufacturing (FDM), fused filament fabrication (FFF), directed ink writing (DIW), and continuous fibre fabrication (CFF) [46–49]. The principle of this method is that the material is melted at a high temperature and ejected from the nozzle; then, the material solidifies quickly after being ejected. (2) 3DP using photography includes stereolithography (SLA), digital light processing (DLP), and continuous liquid interface production (CLIP) [50, 51]. The principle of this method is that the liquid photosensitive resin is sprayed from the nozzle, and the liquid in the target area is irradiated with ultraviolet light, so that the liquid can be rapidly solidified. (3) The 3DP via layer powder bonding includes powder-based 3DP, electron beam melting (EBM), selective laser melting (SLM), selective heat sintering (SHS), selective laser sintering (SLS), and direct metal laser sintering (DMLS) [52–57]. The principle of SLS consists in spreading the first layer of powder, and then, the infrared laser is used to sinter the powder into the desired solid object. The powder bed is preheated a few degrees below the melting temperature of the polymer, and the laser locally provides only the thermal energy necessary to melt the polymer. In addition, the commonly used 3DP techniques also include laminated object manufacturing (LOM) [58],

Table 1: Classifications of 3DP technology [43].

Technical types	Technical names	Materials	Printer manufacturer	Sources
Melt extrusion	Fused deposition manufacturing (FDM)	Thermoplast, eutectic alloy, rubber	Stratasys 3D Systems	[46]
	Fused filament fabrication (FFF)	Thermoplast, eutectic alloy, rubber, etc.		[47]
	Directed ink writing (DIW)	Ceramics, alloy, metal ceramic, etc.		[48]
	Continuous fibre fabrication (CFF)	Nylon, straps, glassfibre, etc.		[49]
Photopolymerization	Stereolithography (SLA)	Photosensitive resin	3D Systems	[51]
	Digital light processing (DLP)	Photosensitive resin		
	Continuous liquid interface production (CLIP)	Photosensitive resin		
Layer powder bonding	Powder-based 3DP	Almost any alloy, powdered polymer, gypsum	Z Corporation 3D Systems Stratasys	[52]
	Electron beam melting (EBM)	Almost any alloy (including titanium alloys)		[53]
	Selective laser melting (SLM)	Titanium alloy, cobalt chromium alloy, stainless steel, aluminum		[54]
	Selective heat sintering (SHS)	Thermoplastic powder		[55]
	Selective laser sintering (SLS)	Hot plastic, metal powder, ceramic powder		[56]
	Direct metal laser sintering (DMLS)	Almost any alloy		[57]
Lamination	Laminated object manufacturing (LOM)	Paper, sheet metal, plastic film	Helisys	[58]
Powder feeding	Directed energy deposition (DED)	Almost any alloy	Fraunhofer	[59]
Metal wire	Electron beam freeform fabrication (EBF^3)	Almost any alloy	LARC	[58]

directed energy deposition (DED) [58, 59], and electron beam freeform fabrication (EBF^3) [58].

The general processes of 3DP technologies are mostly similar and can be divided into four steps: (1) 3DP model building, which usually uses computer-aided design (CAD) software to build a 3D solid model. In this process, the solid 3D model can be built independently or can be acquired using other means such as CT scanning. (2) Model format conversion and slicing. In this process, it is necessary to convert the established 3D model into a format that can be recognized by the 3D printer. Then, the model is sliced according to the accuracy of the 3D printer. (3) The 3DP path and parameter setting to printing. (4) Postprocessing of printed models. For some 3D printed models, redundant materials (such as the supporting materials) may need to be removed after printing.

2.2. The Materials of 3DP. Different 3DP techniques require different materials (Wang and Qi [54]). Table 2 describes the 3DP materials used in different 3DP techniques. Currently, the 3DP materials such as polylactic acid (PLA), gypsum-like materials, photosensitive resins, and acrylonitrile butadiene styrene (ABS) have been used in the production of rock mass specimens [60–64]. The failure of rock materials generally shows high strength and high brittleness. However, from the test data of these materials, the specimens made from these materials exhibit low strength and high ductility which are different from the mechanical and failure characteristics of real rocks. To address this issue, Fereshtenejad and Song [65] investigated the material properties of powder layer printing technique and found that by using appropriate posttreatment techniques and changing printing parameters, the strength of 3DP specimens could be improved. However, the test results still differed from the mechanical and failure properties of natural rocks. Perras and Vogler [66] made specimens with two different particle sizes using the powder layer and inkjet head technology to carry out Brazilian splitting tests. Through comparative testing of three types of natural sandstone specimens, it was found that the specimens made using 3DP were close to the sandstone specimens with the weakest roughness, tensile strength, and fracture processes. Zhou and Zhu [67] compared specimens made of five 3DP materials and conducted mechanical analyses, which found that the photosensitive resin is the most ideal material for building hard and brittle rocks. According to the test results shown in Figure 1, the photosensitive resin specimens printed using stereolithography (SLA) have better strength, but their brittleness characteristics are still less than those of natural rocks. Therefore, the brittleness of the specimens should be improved by freezing at low temperatures and adding internal macro- or microcracks.

2.3. 3D Printers. In addition to the printing materials, the printing equipment is another factor limiting the applications of 3DP in the related fields. In 1986, the first 3DP device (SLA-250) was produced by 3D Systems Corporation. Since then, the 3DP technology has developed rapidly in industrial applications, and the corresponding 3D printers have been developed on the basis of different printing technologies. In 1989, Deckard invented selective laser sintering

Table 2: 3D printed rock specimens.

Materials	Specimen	Description of mechanical properties	Failure properties of specimen	Sources
Sand-based materials		Unconfined compressive strength (UCS) at about 20 MPa Young's modulus at about 1.8 GPa	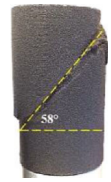	[35] [36] [71] [72]
Resin		Unconfined compressive strength (UCS) at about 80 MPa Young's modulus at about 1.5 GPa		[30, 31] [67]
Gypsum powder		Unconfined compressive strength (UCS) at about 55 MPa Young's modulus at about 7 GPa		[73–76]
Ceramics power		Unconfined compressive strength (UCS) at about 3 MPa Young's modulus at about 0.15 GPa		[67] [77]
Mixed materials		Unconfined compressive strength (UCS) at about 55 MPa Young's modulus at about 5 GPa		[78] [79] [80] [81]
Polylactic acid (PLA)		Young's modulus at about 1.391 GPa		[37]
Acrylonitrile butadiene styrene (ABS)		$K_{IC} \approx 0.789 \pm 0.131$ MPa-m$^{1/2}$ $J_{IC} \approx 256 \pm 84$ J/m^2	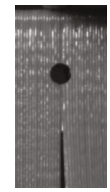	[64]

(SLS), which enabled the application of laser sintering technology in the field of 3DP [68]. In 1995, Z Corporation obtained a license from MIT and produced this type of 3DP device. In 2005, the company also invented the first high-precision colour 3D printer. Subsequently, several printers have been developed and widely used. In 2009, Organovo, USA, used 3DP to manufacture artificial blood vessels. In 2011, Southampton University, UK, printed the first unmanned aircraft using 3DP. In 2011, Kor Ecological Company launched the first car whose surface and parts were manufactured using 3DP. In 2013, British researchers printed embryonic stem cells and similar biological tissues

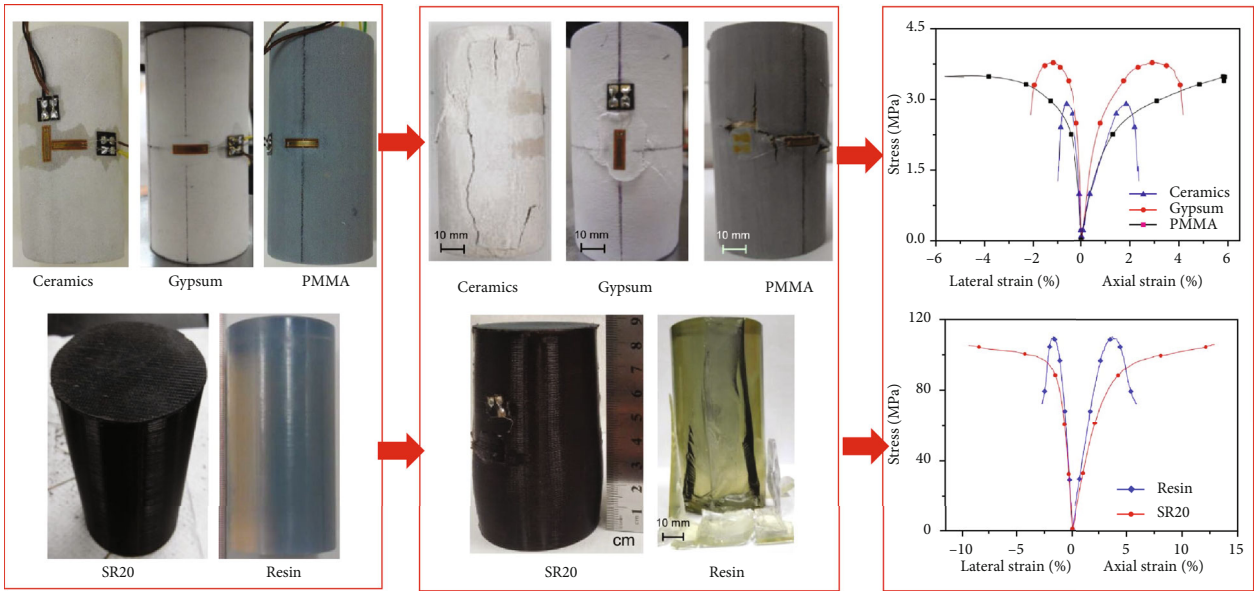

FIGURE 1: Standard specimens prepared using different 3DP materials and their failure modes: (a) standard specimens, (b) failure modes, and (c) stress-strain curves related to the specimens [67].

for the first time with a 3D printer. Since 2014, the 3DP applications in shipbuilding, aerospace science and technology, medicine, construction, automobiles, and other fields have appeared [69, 70].

The current 3D printer manufacturers are mainly located in the United States, Israel, Germany, Japan, Sweden, and other countries. Among them, 3D Systems and Stratasys account for almost 90% of the production of 3D printers. In 2011, 3D Systems acquired Z Corporation, and in 2012, Stratasys acquired Israel's Objet Company and completed resource integration. The current equipment manufacturers corresponding to different 3DP technologies are also listed in Table 1. From Table 1, it can be seen that for 3DP technologies such as FEM, FFF, DIW, and CFF, the related manufacturers of 3D printers are mainly Stratasys and 3D Systems. For 3DP technologies such as SLA, DLP, and CLIP, the main equipment manufacturer is 3D Systems. For 3DP technologies such as powder-based 3DP, EBM, SLM, SHS, SLS, and DMLS, the manufacturers mainly include Z Corporation, 3D Systems, and Stratasys. For LOM, DED, and EBF^3 technologies, the major equipment manufacturers are Helisys, Fraunhofer, and LARC, respectively.

Although there are many kinds of 3DP techniques and printers, the applications of 3DP technology and its materials in rock mass engineering reconstruction are limited because of the following requirements. (1) The natural rocks are generally characterized by high strength; the applications of 3DP in rock mass engineering should meet the high strength conditions. (2) The failure of rock materials is generally brittle. When the rock structure is reconstructed via 3DP, the reconstructed specimens should meet the characteristic of high brittleness. (3) The structure of rock contains joints and cracks, so the corresponding 3DP materials and printers need to meet the characteristics of high precision. (4) It is necessary to obtain the mechanical parameters of rock mass on the engineering scale. Therefore, in order to reconstruct the large size of rock mass specimens, the 3D printer that meets the requirement of printing large-size rock mass is also needed.

3. Applications of 3DP in Rock Mass Experimental Tests

With the development of 3DP technology, it has been preliminarily applied in the field of rock mass engineering. In this section, the use of 3DP in rock mass experimental tests was summarized.

3.1. Preparation of Specimens in Laboratory Tests

3.1.1. Experimental Tests on 3D Printed Specimens. The mechanical and failure properties of 3D printed specimens are the basis for the applications of 3DP technology in rock mass experimental tests. In the process of making rock specimens, some materials are selected to reconstruct the 3DP rock mass. Table 2 describes the 3DP materials used for reconstructing rock specimens and the mechanical and failure properties (such as UCS and Young's modulus) of corresponding materials. As is shown in Table 2, the sandstone-based materials were used to prepare standard size specimens using 3DP [66, 71, 72]. It was found that the uniaxial compressive strength of the specimens was about 20 MPa, and Young's modulus reached about 1.8 GPa. The failure mode exhibits brittle failure characteristics, which is consistent with natural sandstone specimens.

Zhou and Zhu [67] reported that the resin is the most ideal material for simulating rock materials based on the comparison of mechanical and failure properties of five

standard 3DP materials. Therefore, the resin has been used in several studies due to its mechanical and failure characteristics [30–32]. However, the ductility of resin is large, exhibiting plastic characteristics under uniaxial compression, which is different from the brittle failure of rocks. To solve this problem, the brittle failure can be increased by freezing it at low temperatures and adding macro- or microcracks within the specimen [67]. In addition to the sandstone-based materials and photosensitive resin, gypsum has been used in several studies to reconstruct rock specimens using 3DP [73–76]. The 3D printed specimens reconstructed by gypsum generally have low strength, which is suitable for simulating soft rock structures. Wu et al. [73] used glue immersion with evacuation to enhance the rock specimens and achieved better results. The failure characteristics of 3D printed gypsum specimens under uniaxial compression are also presented in Table 2. As can be seen from Table 2, the 3D printed gypsum specimens exhibit brittle failure, which is consistent with the failure of natural rocks. However, the specimens prepared from gypsum have anisotropic characteristics [73]. In addition, since the gypsum specimens need to be soaked with glue to improve their strength, the glue cannot penetrate into the interior of specimens uniformly, leading to the uneven strength of specimens.

Several studies have mixed the cement with printing materials when preparing the 3D printed specimens. For example, as is shown in Table 2, Feng et al. [78] printed the specimens using 525R ordinary Portland cement and obtained the mechanical and failure characteristics of the specimens under uniaxial compression. The uniaxial compressive strength of specimens reached 60 MPa, and the elastic moduli reached about 5 GPa. For the failure characteristics of 3D printed specimens prepared from this material, the brittle failure was predominant. Like the 3D printed specimens prepared using gypsum, the specimens are anisotropic which can be used to simulate the mechanical and failure characteristics of shale.

3.1.2. Repetitive Preparation of Rock Mass with Complex Structures. Since the 3DP has the characteristics of high precision and repeatability, it has been used in the preparation of specimens containing different structures. The mechanical and failure characteristics of the same structural specimens under different mechanical conditions were tested on this basis. Compared with the traditional laboratory specimens containing joints and fissures, the 3DP method allows for the repetitive preparation of rock specimens with the same structures. For example, several studies have used 3DP methods to prepare specimens with single and multiple fractures and studied the mechanical and failure properties of rock specimens under different loading conditions (Table 3) [82–85].

The reconstruction of rock masses requires higher precision because of the influence of mechanics and structure on the failure process. Compared with traditional rock mass reconstruction methods, the 3DP has the advantages of higher precision and efficiency. Therefore, the repeatability of 3D printed specimens is better than that of specimens prepared by traditional methods, which makes it easier to analyze the effects of different external factors (e.g., rock structure, surrounding pressure state, and loading conditions) on the failure characteristics. For example, the mechanical properties of structural planes in rock masses are related to geological disasters such as landslides and rock bursts, which play an important role in the safety and stability control of rock mass engineering. Therefore, the determination of the mechanical properties of rock mass structural planes is the basis of rock mass engineering design, construction, and stability evaluation. The repetitive preparation of identical specimens containing structural planes is the factor for studying the mechanical and failure characteristics of rock masses [88]. Compared with the regularity of joints and fissures prepared in the laboratory, the natural joint planes have irregular characteristics, so it is difficult to prepare the representative specimens in experiments. Moreover, it is hard to obtain the failure and mechanical characteristics of the same structural planes under different mechanical conditions.

Due to the advantages of 3DP technology, such as the high precision and reproducibility, several studies have attempted to use 3DP to prepare identical rock mass specimens containing structural surfaces. Table 4 presents the typical cases of rocks containing structural planes produced by 3DP technology. Ban et al. [89] printed the scanned data of structural planes using 3DP and then achieved the repetitive production of natural structural planes. The advantage of this method is that they used 3DP as the bridge of obtaining structural plane information and repetition reconstruction. However, the mechanical similarity between natural rocks and casting materials should be considered. Ishibashi et al. [90] used acrylic resin to produce the 3D printed shear specimens with specific roughness coefficients. The tests results showed that the 3DP is an effective method for producing structural planes with specific roughness coefficients. Specifically, it allows for the repeated tests on the shear seepage characteristics of identical rock mass specimens.

The main advantage of 3DP is the precise reconstruction of complex structures. Taking advantage of this, several studies have used 3DP to reconstruct the rock masses with complex structures. Suzuki et al. [92, 93] produced the rock mass specimen containing complex fracture networks using 3DP (Figure 2). The analysis of CT scanning results revealed that the rock mass specimens reconstructed using 3DP reduced the uncertainty of laboratory tests and numerical calculations, which are important for the acquisition of mechanical and failure characteristics of complex fractured rock masses.

In rock mass engineering, understanding the mechanical and failure characteristics of complex structural rock masses is the basis of engineering safety design, analysis, and stability evaluation. The structure of rock mass is the controlling factor that determines the mechanical and failure characteristics. However, it was difficult to reconstruct structural rock masses for either experimental testing or numerical calculations. Xia et al. [43, 44] used 3DP to reconstruct the columnar jointed rock mass at Baihetan hydropower station (Figure 3). By comparing the mechanical properties, failure characteristics, and acoustic emission characteristics of the

Table 3: 3DP fractured rock specimens.

No.	Specimen	Specimen materials and test conditions	Test results	Relevant mechanical parameters	Comments	Sources
1		Photosensitive resin Dynamic loading		Dynamic compressive stress and strain, longitudinal wave velocity, elastic modulus, etc.	Symmetrical wing cracks initiated The specimen cannot completely reflect the mechanical behavior of brittle rocks	[86]
2		Photosensitive resin Static uniaxial compression		Compressive strength and axial strain at the peak stress influenced by the flaw number and angles.	Wing and antiwing cracks wrapped around the flaw edge The maximum crack propagation velocity in single flawed specimens is higher than that in double flawed specimens	[87]
3	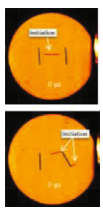	Gypsum-like material Dynamic loading	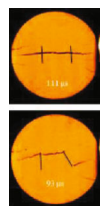	Dynamic compressive stress and strain, longitudinal wave velocity, elastic modulus, etc.	The 3DP technique could prepare specimens with preset cracks The failure patterns of gypsum-like specimens are close to the rock mechanical tests	[40]
4		Gypsum-like material Brazilian tests	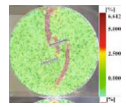	Young's modulus, Poisson's ratio, uniaxial compressive strength, tensile strength.	3D printed rock-like Brazilian discs with preexisting flaws were investigated The 3DP technology combined with DIC method shows the superiority in the laboratory test	[82–84]

Table 4: 3D printed natural structural planes.

No.	Specimen	Specimen material and target test	Test type	Specimen preparation	Sources
1		Polylactic acid Shear tests	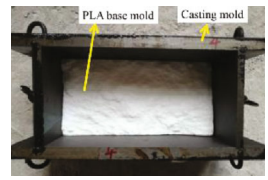	Scanning of natural rock mass structural plane using 3D scanning technology The information on the structural plane of the natural rock mass was printed and used as a mold, and the repetitive pouring of the structural plane was achieved on this basis	[89]
2	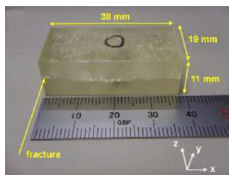	Acrylic resin Shear tests	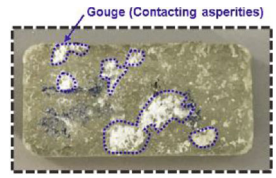	Acrylic resin was used to prepare the structural plane, and shear tests were carried out	[90]
3		Polylactic acid Shear test		3DP method was used to make the shear sample mold, and then, the sample was poured	[91]

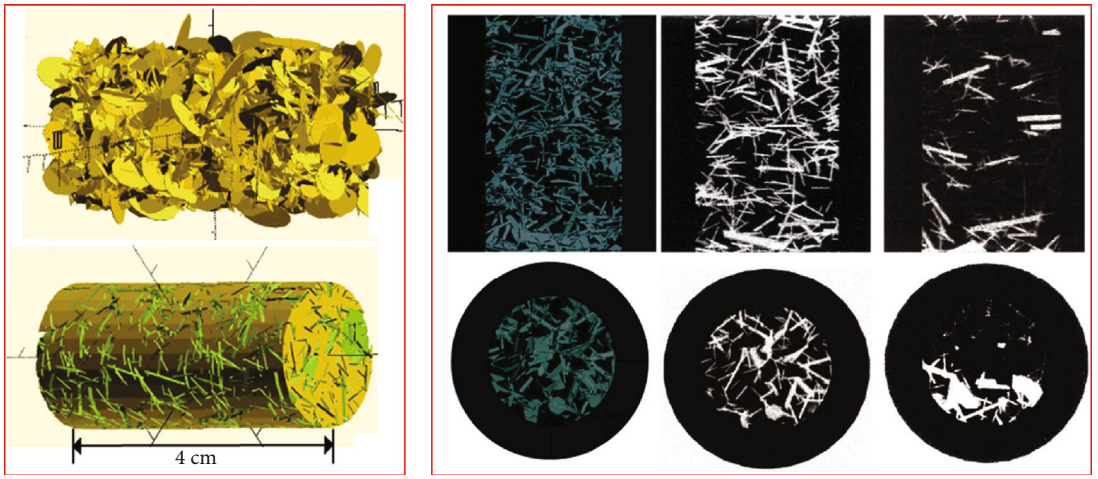

Figure 2: Precise reconstruction of complex rock mass structures using 3DP [92, 93]: (a) 3DP preparation of complex rock mass structures; (b) CT scanning results of the 3D printed rock specimens.

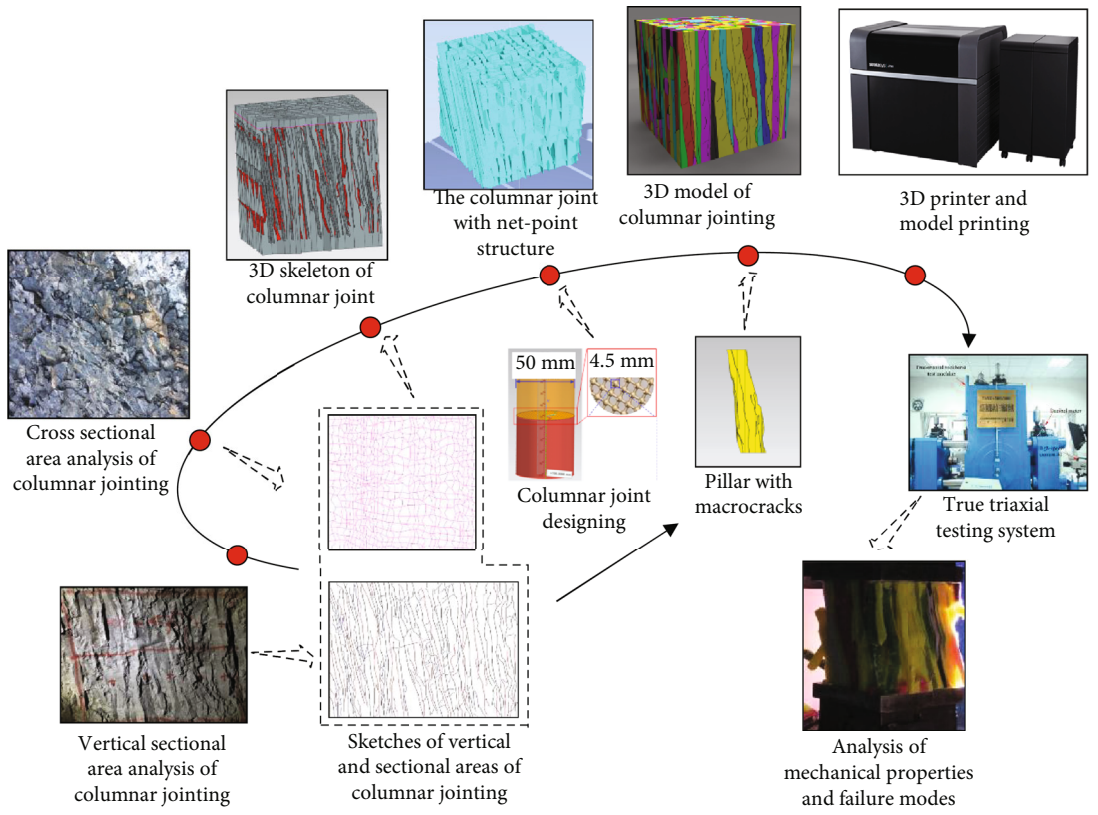

Figure 3: Accurate reconstruction of columnar jointed rock mass using 3DP [44].

3DP reconstructed columnar jointed rock mass with the results of in situ and laboratory tests, the mechanical properties of the 3DP reconstructed columnar jointed rock mass were verified, which demonstrates the effectiveness of 3DP in the structural reconstruction of complex rock masses.

The accurate description and visualization of complex internal structures and stress distribution of rock mass are important for solving the various underground engineering problems [30]. By comparing stress and failure characteristics of the 3DP reconstructed model with natural coal specimens, the discontinuity and stress freezing technique can be intuitively quantified by the combined application of 3DP and CT scanning (Figure 4). The method of combining 3DP with the stress freezing technique is a promising method for quantifying and visualizing the complex fracture structures of underground rock masses and their influences

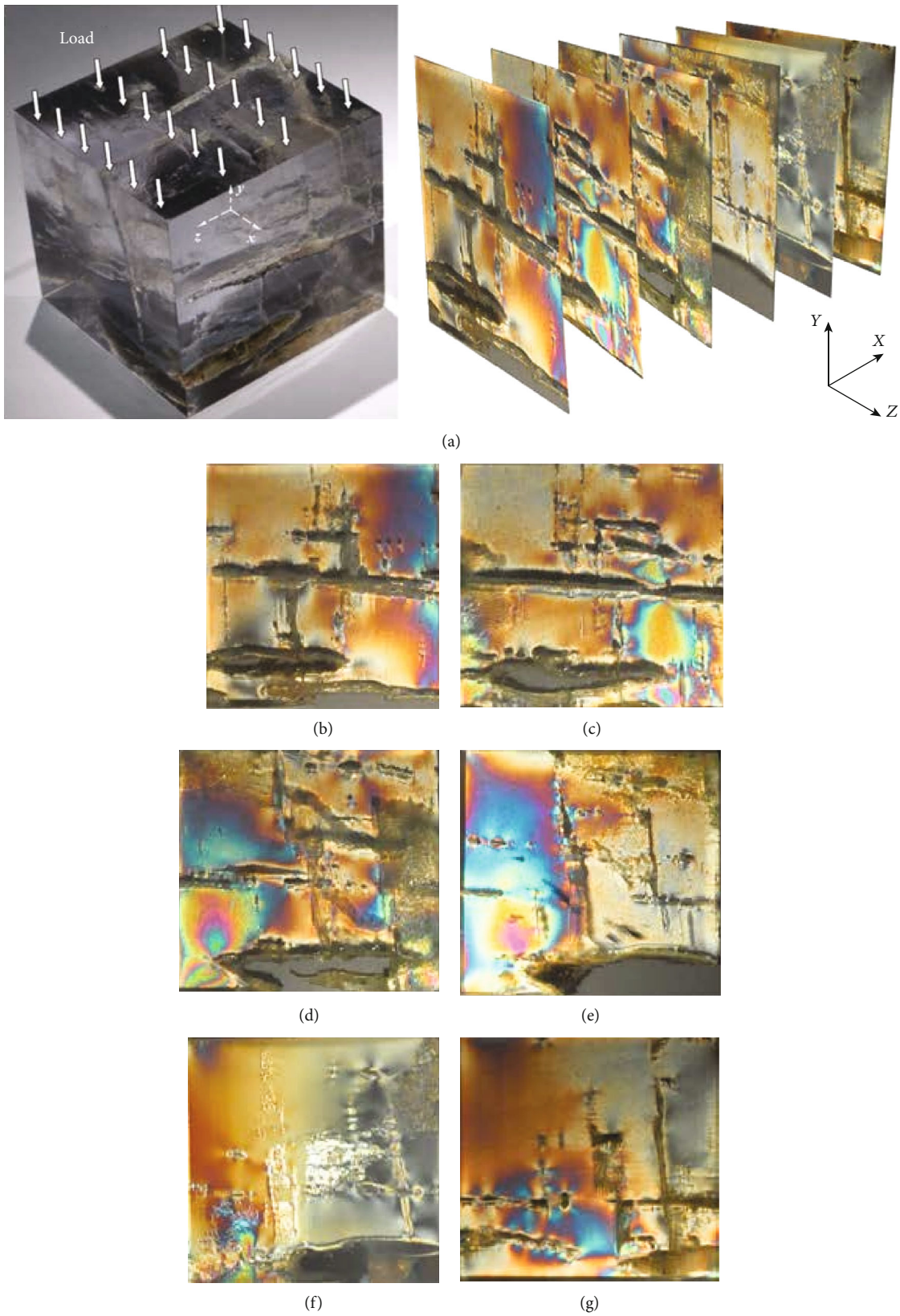

Figure 4: Accurate reconstruction of fractured rock mass using 3DP [30].

Figure 5: Failure processes of the 3D printed twin-hole tunnel [105].

on the 3D stress distribution. In addition, this method can also be used to verify the numerical simulation results.

3.2. Tunnel Failure Simulation. Geomechanical model tests can accurately reflect the spatial relationship between engineering geology and the structure of rock mass. The test results can provide an intuitive interpretation of mechanical properties, deformation trends, and stability characteristics of rock masses. Therefore, the experimental tests have become an important method for studying the stability of rock structures and verifying numerical simulations [74, 94–96]. In deep underground projects, there are widely adjacent tunnels and caverns, such as the twin railroad tunnels for urban and mountain highways [97–100], large caverns in hydroelectric power plants [101, 102], and the deep mine tunnels [103, 104]. The quantitative stability evaluation of multitunnel structures is an important issue related to the safety evaluation and stable construction of underground tunnels. Jiang et al. [105] simulated the overall failure process of the twin-tunnel structure based on a 3D printed sandstone reconstruction model (Figure 5). In addition, they proposed the safety factor method for evaluating the overall

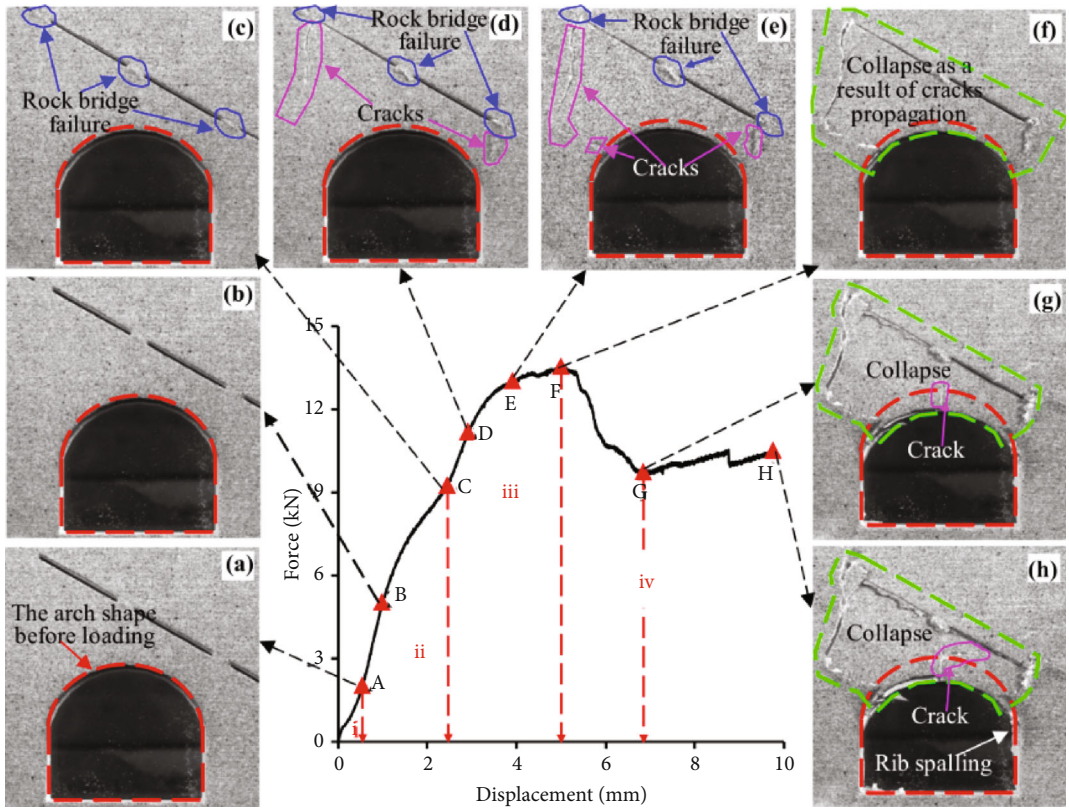

Figure 6: Failure processes of the 3D printed tunnel model [74].

safety of multitunnel structures. The experimental results and corresponding numerical analysis showed that the reconstruction of the twin-tunnel structure using 3DP is an effective method for studying tunnel failure and stability analysis. It was determined that for the double tunnel structures, the plastic strain connectivity between tunnels can be used as a conservative instability criterion, and the tunnel displacement inflection point can be used as the overall instability criterion, respectively.

The repetitive preparation of tunnel models and mechanical testing are some of the most commonly used research methods for studying tunnel stability [106–108]. However, the preparation of rock specimens using traditional methods has disadvantages, including time-consuming and unavoidable human errors [30]. The reconstruction method of 3DP may overcome the disadvantages of traditional geotechnical modelling methods. Song et al. [74] prepared four tunnel models via 3DP with gypsum powder and PLA (polylactic acid) materials. The uniaxial compression test results showed that the failure characteristics of the conventional tunnel and single fault tunnel models are similar to the failure process of the 3D printed model (Figure 6). The results of the experimental tests are in general agreement with the artificial model tests, tunnel engineering examples, and numerical simulations, indicating that the 3DP technology can be applied to the experimental study of tunnels.

3.3. Integration of the 3DP with Other Techniques. As the new technique, the 3DP can be combined with other advanced techniques in the failure analysis of rock masses, thus making up for the disadvantages of traditional testing methods. This section focuses on the applications of 3DP in the combination with other related techniques.

3.3.1. Integration of 3DP with 3D Scanning and CT Scanning. The mechanical properties of structural planes are the important factors affecting the stability of rock mass. Therefore, the typical strength of structural planes has been concerned in the field of rock mechanics [109–113]. However, the structural planes of the natural rock masses are complex, and the morphology is characterized by anisotropy and size effects. So, it is difficult to accurately evaluate the shear strength of natural structural planes.

In the traditional experimental tests, since it is difficult to make irregular rock mass structures in the preparation processes, the specimen needs to be simplified. The influences of irregular rock mass structures on the mechanical and failure characteristics are ignored, which makes the mechanical characteristics of rock mass differ from the test results. With the development of measurement technology, several studies have applied digital photogrammetry methods to rock mass structure measurements [115–119]. In particular, 3D laser scanners can achieve real replication and are now gradually being used in the field of engineering measurements and detection. The 3D laser scanner can obtain 3D information for complex, irregular, and nonstandard objects. So, it has become an important method for obtaining information on the irregular structures of rock masses [114]. As is shown in Figure 7 [114], the surface information for irregular rock structures was acquired via

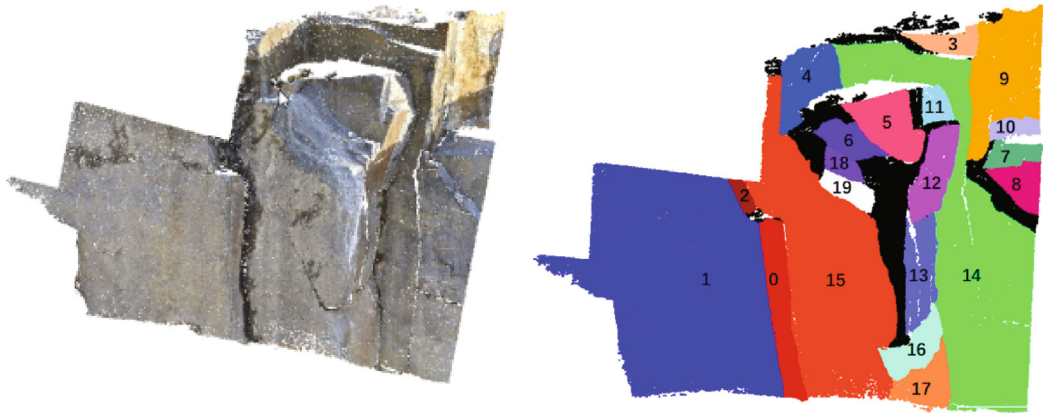

(a) (b)

Figure 7: Acquisition of 3D scanning data for rock masses [114]: (a) photographs of natural rock mass structures and (b) the 3D information of rock masses regenerated by postprocessing point cloud data.

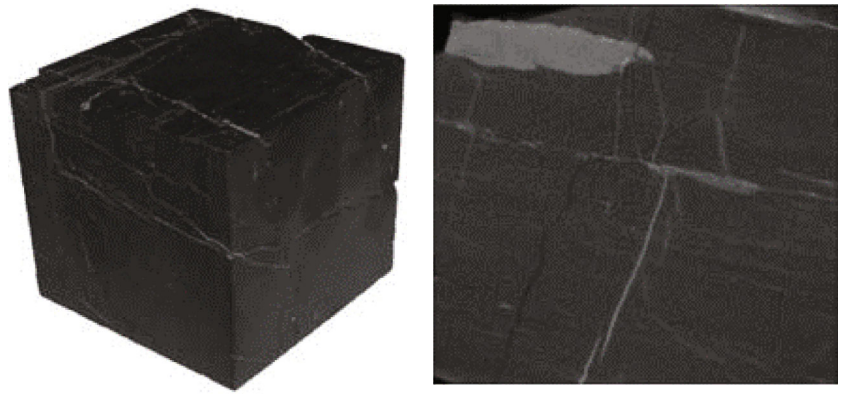

(a) (b)

Figure 8: Acquisition of CT scanning data for rock masses [30].

3D scanning, and the 3D data for rock masses was regenerated by postprocessing point cloud data. Then, the data can be output by the 3DP printer, which solved the problem of an irregular rock mass structure that cannot be reproduced by general methods of laboratory tests.

In addition to the surface irregularities, defects such as joints and fissures also exist within rock masses [120–122]. Nondestructive CT identification can be used to obtain images of internal structures of rock mass under different environments without disturbance. The CT images are expressed as the colour of CT number, which finally reflects the distribution of each medium inside rocks. The CT technique can be used to obtain the information of joints and fissures inside rock masses (Figure 8) [30]. Therefore, through the combination of CT scanning and 3DP, the irregular joints and fissures can be replicated, and the mechanical properties of the same rock masses under different stress conditions can be obtained.

3.3.2. Integration of 3DP and Numerical Simulations. The 3DP can transform digital models of rock masses into experimental models, thus providing the possibility of repeated failure tests on the complex structure of rock mass. Similarly, the 3D digital models can also be imported into the numerical software for numerical calculations, such as the finite element [123–125] and discrete element [126] analysis. Therefore, the 3DP is compatible with the laboratory tests and numerical simulations and can be regarded as a virtual bridge connecting laboratory tests and numerical simulations. For example, the 3DP was used to verify the reliability of numerical methods [76]. In addition, the 3DP in combination with numerical simulation has focused on the verification of mechanical and failure modes of rock mass specimens (Figure 9) [85].

By comparing the results of uniaxial compression and Brazilian splitting tests of 3D printed specimens with numerical results, it was concluded that the failure mode of specimens produced using 3DP is consistent with the classical numerical simulations. Furthermore, several studies have used a combination of 3DP and numerical simulation to verify the results of laboratory tests, thus demonstrating the effectiveness of 3DP in studying failure modes of rock masses [76, 85].

Since the 3DP can transform digital models of rock masses into laboratory specimens, its main advantage lies in the accurate reconstruction of complex rock mass

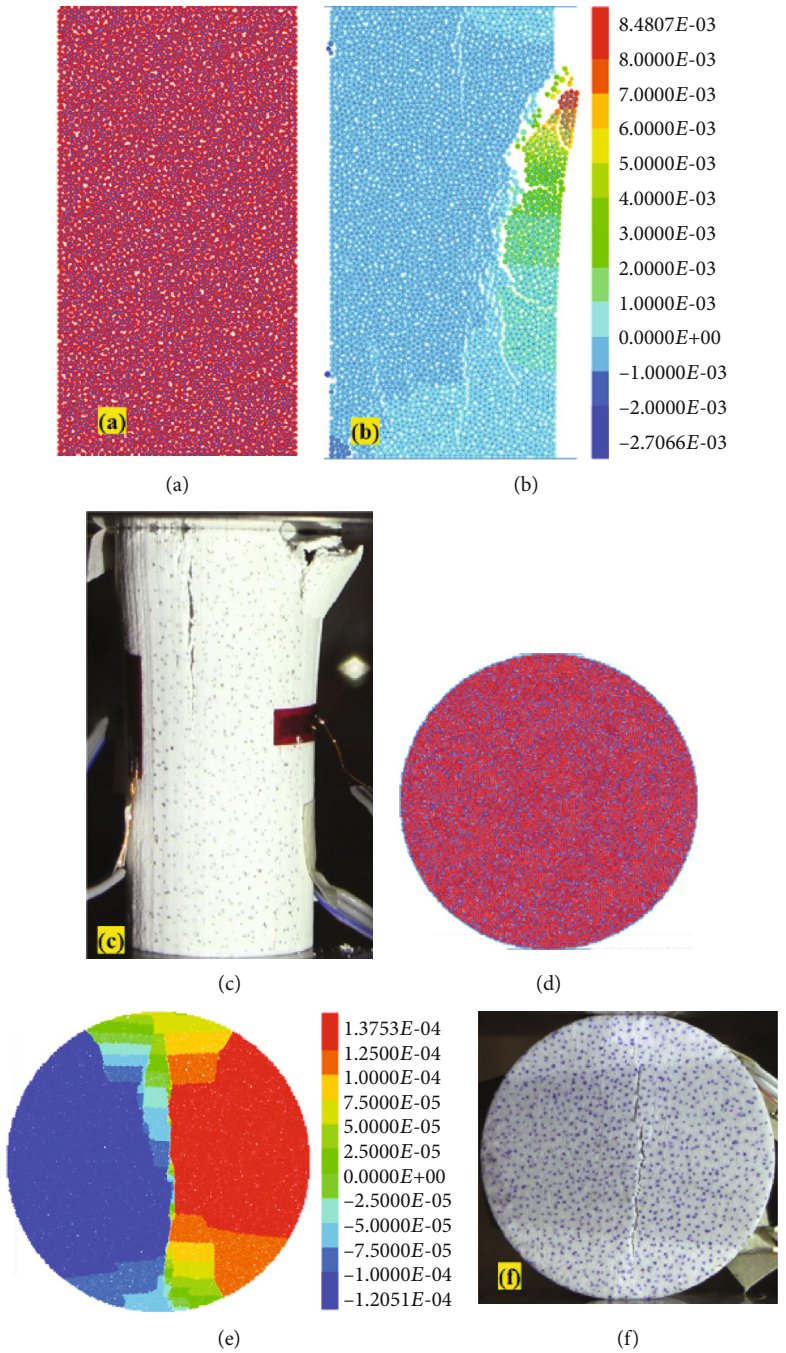

Figure 9: Mutual verification of test results for 3D printed specimen and numerical test [85].

structures. Based on this, Song et al. [74] and Jiang et al. [105] produced tunnel models using 3DP and carried out numerical simulations for comparison. The numerical results are shown in Figure 10. As can be seen in this figure, the combination of 3DP and numerical analysis enabled the thorough analysis of strength, deformation, and failure mode of the rock mass' structure.

3.3.3. Integration of 3DP and the Stress Freezing Technique. The stress freezing technique is an effective method for quantitatively analyzing the three-dimensional stress field within a complex solid structure. The property of isotropic stress or isotropic stripes caused by external loads in a warmed environment can be "frozen" and recorded when the specimen returns to room temperature [30, 126–128]. With the development of optical mechanics experimental technologies, the solid 3D stress freezing method has been used to make progress in the photoelastic material properties, model preparation, 3D optical measurement theory, fringe picking and resolution analysis, and free-surface stress measurements [129–133]. It is a convenient, economical, and effective way to intuitively and quantitatively analyze

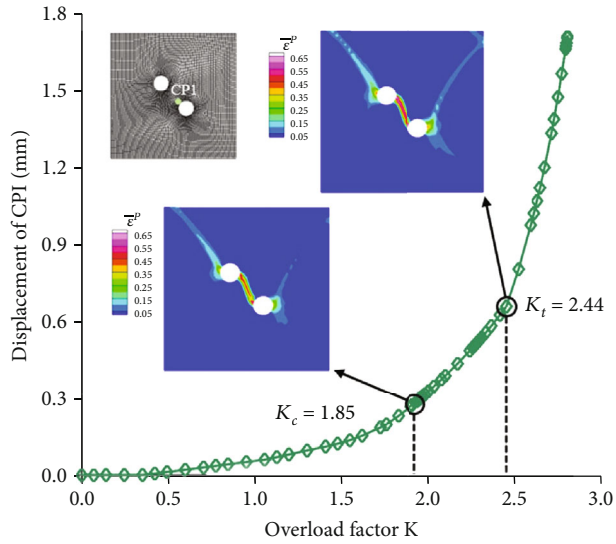

Figure 10: Mutual verification of test results for 3DP rock tunnel model and numerical test: (a) verification of double-hole tunnel and numerical results [105] and (b) verification of numerical results of the tunnel model with a structural plane [74].

the complex stress field in the solid structure. However, the traditional method of model preparation in 3D photoelastic analysis is mainly making the mold and then casting and molding. This method not only requires the solving of casting process challenges but also leads to high costs and long preparation cycles. For the complex solid structures, when using traditional methods to make 3D photoelastic models, the complex local features have to be omitted. In particular, the complex structures within a solid are difficult to set up using conventional methods. For example, it is difficult to prepare photoelastic models of subsurface rock mass media with internal pores or fractures. Therefore, it prevents the 3D stress freezing method from being used to visually display the internal stress field of complex solid structures.

The 3DP technology has enabled the rapid production of complex 3D solid models. Based on the digital model of files,

the 3DP technology uses powdery (or liquid) photosensitive resin, ceramic, or metal materials to build a 3D solid via rapid laser curing and layer-by-layer spraying [134–138]. Compared with the traditional photoelastic material of epoxy resin, the photosensitive resin has similar composition, photoelasticity, and stress freezing characteristics, which ensures the feasibility of making photoelastic models of complex structures with 3DP technology. Therefore, the applications of 3DP and 3D stress freezing methods provide a promising path for realizing the quantitative characterization and visualization of complex analyses. The typical test results obtained using 3DP and stress freezing technique are shown in Figure 11 [31].

3.3.4. Integration of 3DP and Other Electronic Technologies. The numerical and laboratory tests have been used to investigate the factors influencing the mechanical properties of anchored rock joints [139, 140]. Feng et al. [29] used 3DP rock bolts and anchoring glue to reinforce the specimens with joints. The surface morphology of the 3DP rock bolt is consistent with the actual rock bolt with better strength. In addition, the digital image correlation (DIC) method was used to capture the changes of strain/displacement fields of the specimen, and the effects of joint planes and joint angles on the crack process, DIC variation pattern, and stress-strain evolution were discussed in conjunction with the test results.

The scanning electron microscope (SEM) is a high-resolution electrooptical instrument used for observing the microscopic fields of objects [141–143]. The micromorphology of the sample surface can be observed, and this method has been used in the experimental fields because of its high scanning resolution [144–148]. By combining the technologies of 3DP and SEM, the mesostructural features of the 3DP reconstructed rock mass specimens can be obtained. Then, the mesostructural features of the 3DP reconstructed rock mass specimens can be compared with those of natural rock mass structures. It ensures the consistency between the macrostructural features and natural rock mass structures and also describes the structural features of 3D printed specimens on the mesoscale, thus measuring the structural features of rock mass from macroscale to microscale.

4. Discussions

4.1. Improvement of Rock Mass Experimental Methods Using 3DP. As was previously mentioned, the main methods of testing the mechanical properties of jointed rock masses are in situ testing, laboratory tests, and numerical simulations. There are mutual influences and verifications among the three methods [149–153]. In situ testing is the most effective method of obtaining the mechanical parameters of rock masses in engineering. But it takes a long time and is expensive. In addition, in situ testing is mainly used for verification, while laboratory tests are used to obtain the mechanical characteristics of rock masses. Moreover, there are problems such as size effects and anisotropy between in situ and laboratory tests. Due to the limitations of experimental testing equipment such as the size of the rock specimen and the difficult preparation of complex rock mass structures, it is impossible to accurately obtain the change rule of the mechanical properties of the same rock masses under different mechanical conditions. Thus, the reconstruction of complex rock masses has become the bottleneck of obtaining the mechanical parameters of complex rocks. Numerical simulation analysis has the advantages of low cost and repeatability, which are generally used to supplement the in situ and laboratory tests. However, the numerical processes are always limited by the computational model, selection of material parameters, constitutive relationship, etc.

Based on the discussions above, it is clear that the in situ testing, laboratory tests, and numerical simulations mutually validate and support each other. However, due to the limitations of laboratory tests and numerical simulations, there are problems of producing physical and numerical models, which make the obtained physical and numerical model structures differ from the actual rock masses. With the development of 3DP, the methods of obtaining physical and numerical models have been changed (Figure 12). As can be seen from Figure 12, due to the emergence of the 3DP and other techniques, a bridge has been created between in situ tests, laboratory tests, and numerical simulation. Based on the geological surveys and in situ testing of rock masses, the information on the surface and internal structures can be obtained via 3D scanning and CT scanning. Through the digital reconstruction of model structure, the 3DP can be used to output the reconstructed digital model. Thus, a physical model of rock mass with completely consistent structures can be made. Based on this, the mechanical and failure tests can be conducted on identical specimens. Similarly, the reconstructed digital model of rock mass can be imported into the numerical software for calculations. Thus, more accurate mechanical parameters for the engineering design can be obtained by comparing the results of in situ tests, laboratory tests, and numerical simulations. After the comparison, the obtained mechanical parameters can be corrected through the feedback analysis of designing and construction.

4.2. Problems and Challenges regarding the 3DP Technology. Although the 3DP technology has obvious advantages in the reconstruction of rock mass structures, there are still several challenges in the applications of engineering. In this section, we describe the problems that need to be solved.

4.2.1. The 3DP Materials. Rock mass failure has the typical characteristics of high strength, high brittleness, and low ductility. But there is no 3DP material that can satisfy all of these characteristics. Currently, the materials that can be used for 3DP of rock mass structures mainly include photosensitive resin, gypsum, and sandstone-based self-made materials [43, 44]. The rock specimens prepared from these materials often possess one or two of the mechanical and failure characteristics of the real rocks. For example, photosensitive resin is a liquid material before printing. The rock specimens prepared from these materials can meet the characteristics of high strength and precision. However, the

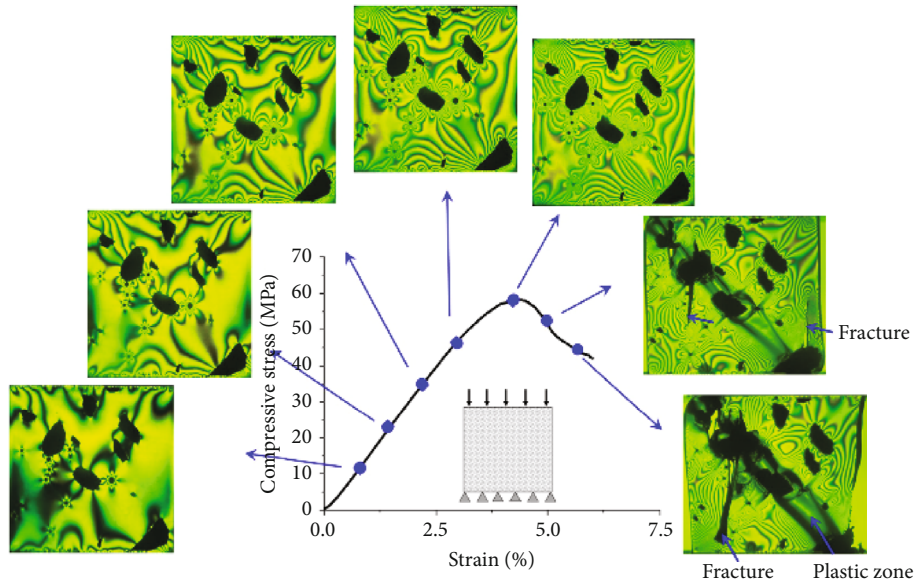

(a)

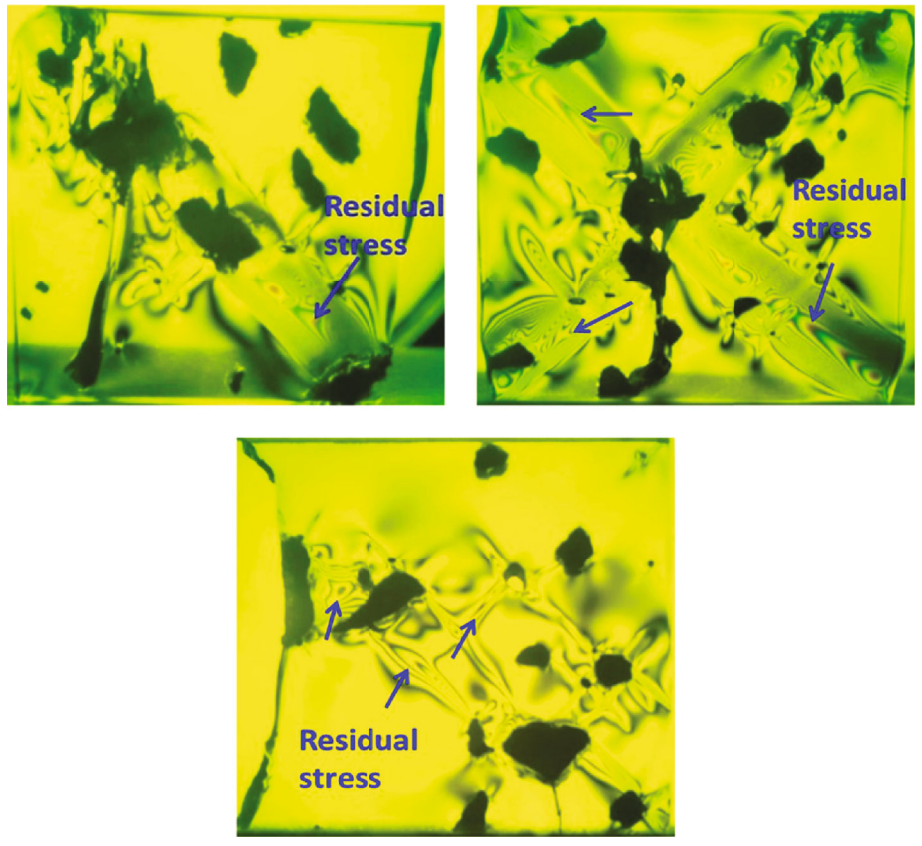

(b)

Figure 11: Applications of 3D printed structures combined with stress freezing technique: (a) monochromatic illumination of the isochromatic fringe pattern of M-III at different loading stages and (b) illustration of the residual stress distribution of the specimens after the removal of the compressive stress [31].

problems of ductility and low brittleness lead to the need for additional treatment [67]. For example, the 3D printed specimen made of gypsum has high brittleness during the failure process, but the strength does not meet the requirements of general rocks [73]. The sandstone-based material specimen is brittle, but the strength differs from those of natural rocks [35].

In terms of the limitations of 3DP materials regarding the mechanical and failure characteristics of rocks, the solution is to modify one material that meets the requirements of

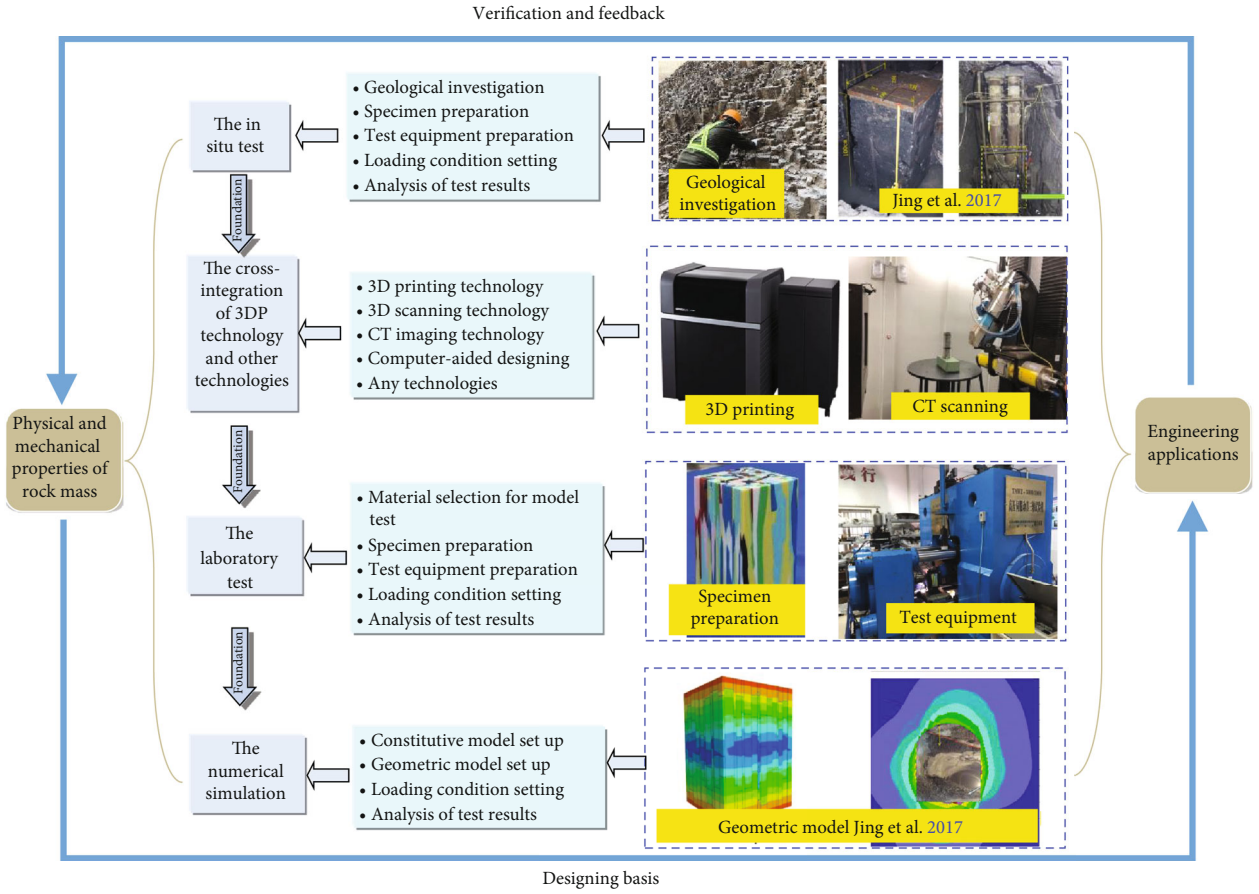

Figure 12: Method changes of obtaining mechanical properties of rock mass by 3DP.

the natural rock masses. For example, photosensitive resin can be modified by adding materials with high brittleness characteristics in order to obtain the characteristics of high brittleness, low ductility, and high strength. But it requires the intersection of geotechnical engineering, chemical engineering, and other related subjects.

4.2.2. The 3D Printers. The 3D printers and printing materials are closely related. Due to the different 3DP processes, most 3D printers can print using one or two types of materials. Therefore, it is necessary to develop 3D printers that can utilize a wide range of 3DP materials. In addition, the 3D printers are relatively expensive, and most researchers cannot afford them, which is one of the main factors that limit the application of 3DP to the accurate reconstruction of rock mass structures.

Since the material of 3DP is accumulated layer by layer in an incremental manner, the preparation of complex structures can be achieved. Thus, making the reconstructed structure anisotropic is one main characteristic but unavoidable. In addition, the defects such as joints and fissures in the rock mass are generally small in size. In order to achieve the accurate reconstruction of these structures, the 3D printers need to have high precision. Therefore, in the aspects of reducing anisotropy of 3D printed specimens and meeting the requirements of preparing small joints and fissures, the 3D printers need to have the property of high precision.

The size effect is a basic feature for the jointed rock masses. To obtain more accurate mechanical parameters of jointed rock masses and to meet the relevant requirements for engineering design, it is necessary to reconstruct the 3D printed models to be a large size in the model tests. This imposes the requirements on the printing size and capability of the 3D printers. First, since the 3D printed specimens need to meet the requirements of large size, it needs to have the capability of printing large specimens. Second, due to the contradiction between the overall size of the modelled rock mass structure and its small structures such as joints and fissures, the 3D printer also needs to be able to produce large specimens containing small structures. Third, due to the large size and high precision requirements of the 3DP, it requires the 3D printer to have long-term printing capability. Overall, these are the main bottlenecks that limit the applications of 3DP technology in rock engineering. With the development of the 3DP technology, those problems can be solved, and the 3DP technology will be widely used in rock mass engineering.

5. Conclusions

In this paper, the technical development, equipment situation, application fields, and challenges involved in using 3DP technology in rock mass mechanics were

comprehensively reviewed, and the following conclusions were obtained.

(1) As an emerging technology, the 3DP has obvious advantages in terms of the production of experimental rock models compared to previous sample preparation techniques. This technology has been used in the precise reconstruction of rock mass structures. The results of the 3D printed specimens used in uniaxial compression show that the 3DP has broad application prospects in the geotechnical engineering

(2) The 3DP technology has been successfully applied in the specimen preparation for laboratory tests and repetitive preparation of natural rock masses containing structural planes. By combining the technology of 3DP with 3D scanning, CT scanning, numerical calculations, stress freezing technique, and other advanced techniques, the complex structural rock masses can be accurately reconstructed. Based on this, the mechanical and failure characteristics of the identical rock masses under different mechanical boundary conditions can be obtained

(3) The mechanics and failure modes of the general rock specimens have the characteristics of high strength, high brittleness, and low ductility. However, the 3DP materials containing all of those above characteristics have not yet been developed, which has become the main constraint in the use of 3DP in the geotechnical engineering

(4) Due to the size effect of rock masses and anisotropic characteristics of the 3D printed specimens, it is necessary for the 3D printers to have high precision, be able to print large specimens, be suitable for long-term printing, and have the capability to print using different types of materials

Data Availability

All data, models, and code generated or used during the study appear in the submitted article.

Conflicts of Interest

The authors declared that they have no conflicts of interest in this work. We declare that we do not have any commercial or associative interest that represents a conflict of interest in connection with the work submitted.

Acknowledgments

The study was funded by the National Natural Science Foundation of China (Grant Nos. 42077251, 41807269, and U1865203). The work presented in this paper was also supported by the Open Research Fund of State Key Laboratory of Geomechanics and Geotechnical Engineering, Institute of Rock and Soil Mechanics, Chinese Academy of Sciences (Grant No. Z020011), and Fundamental Research Funds for the Central Universities (Grant No. DUT20RC(3)011).

References

[1] Y. H. Hatzor, X. T. Feng, S. J. Li, G. Yagoda-Biran, Q. Jiang, and L. X. Hu, "Tunnel reinforcement in columnar jointed basalts: the role of rock mass anisotropy," *Tunnelling and Underground Space Technology*, vol. 46, no. 1, pp. 1–11, 2015.

[2] H. L. Tu, C. S. Qiao, and Z. M. Han, "Elastic-brittle-plastic analysis of the radial subgrade modulus for a circular cavity based on the generalized nonlinear unified strength criterion," *Tunnelling and Underground Space Technology*, vol. 71, pp. 623–636, 2018.

[3] X. Wang, W. Yuan, Y. Yan, and X. Zhang, "Scale effect of mechanical properties of jointed rock mass: a numerical study based on particle flow code," *Geomechanics and Engineering*, vol. 21, no. 3, pp. 259–268, 2020.

[4] Y. Zheng, C. X. Chen, T. T. Liu, and Z. H. Ren, "A new method of assessing the stability of anti-dip bedding rock slopes subjected to earthquake," *Bulletin of Engineering Geology and the Environment*, vol. 80, no. 5, pp. 3693–3710, 2021.

[5] W. Q. Mu, L. C. Li, T. H. Yang, G. Yu, and Y. Han, "Numerical investigation on a grouting mechanism with slurry-rock coupling and shear displacement in a single rough fracture," *Bulletin of Engineering Geology and the Environment*, vol. 78, no. 8, pp. 6159–6177, 2019.

[6] W. Q. Mu, L. C. Li, T. H. Yang, L. J. Yao, and S. X. Wang, "Numerical calculation and multi-factor analysis of slurry diffusion in an inclined geological fracture," *Hydrogeology Journal*, vol. 28, no. 3, pp. 1107–1124, 2020.

[7] T. Xu, T. F. Fu, M. J. Heap, P. G. Meredith, T. M. Mitchell, and P. Baud, "Mesoscopic damage and fracturing of heterogeneous brittle rocks based on three-dimensional polycrystalline discrete element method," *Rock Mechanics and Rock Engineering*, vol. 53, no. 12, pp. 5389–5409, 2020.

[8] Y. J. Yu, W. C. Zhu, L. C. Li, C. H. Wei, B. X. Yan, and S. Li, "Multi-fracture interactions during two-phase flow of oil and water in deformable tight sandstone oil reservoirs," *Journal of Rock Mechanics and Geotechnical Engineering*, vol. 12, no. 4, pp. 821–849, 2020.

[9] W. J. Darlington, P. G. Ranjith, and S. K. Choi, "The effect of specimen size on strength and other properties in laboratory testing of rock and rock-like cementitious brittle materials," *Rock Mechanics and Rock Engineering*, vol. 44, no. 5, pp. 513–529, 2011.

[10] Y. X. Xiao, X. T. Feng, B. R. Chen, G. L. Feng, Z. B. Yao, and L. X. Hu, "Excavation-induced microseismicity in the columnar jointed basalt of an underground hydropower station," *International Journal of Rock Mechanics and Mining sciences*, vol. 97, no. 9, pp. 99–109, 2017.

[11] Y. J. Xia, L. C. Li, C. A. Tang, X. Y. Li, S. Ma, and M. Li, "A new method to evaluate rock mass brittleness based on stress-sestrain curves of class I," *Rock Mechanics and Rock Engineering*, vol. 50, no. 5, pp. 1123–1139, 2017.

[12] G. Herget and K. Unrug, "_In situ_ rock strength from triaxial testing," *International Journal of Rock Mechanics and Mining sciences and Geomechanics Abstracts*, vol. 13, no. 11, pp. 299–302, 1976.

[13] Q. Jiang, X. T. Feng, J. Chen, K. Huang, and Y. L. Jiang, "Estimating *in-situ* rock stress from spalling veins: a case study," *Engineering Geology*, vol. 152, no. 1, pp. 38–47, 2013.

[14] F. K. Nizametdinov, A. A. Nagibin, V. V. Levashov, R. F. Nizametdinov, N. F. Nizametdinov, and A. E. Kasymzhanova, "Methods of in situ strength testing of rocks and

joints," *Journal of Mining Science*, vol. 52, no. 2, pp. 226–232, 2016.

[15] K. Kovari, A. Tisa, and H. H. Einstein, "Suggested methods for determining the strength of rock materials in triaxial compression: revised version," *International Journal of Rock Mechanics and Mining Sciences and Geomechanics Abstracts*, vol. 20, no. 6, pp. 285–290, 1983.

[16] J. Yu, W. Yao, K. Duan, X. Y. Liu, and Y. L. Zhu, "Experimental study and discrete element method modeling of compression and permeability behaviors of weakly anisotropic sandstones," *International Journal of Rock Mechanics and Mining sciences*, vol. 134, no. 10, article 104437, 2020.

[17] R. E. Goodman, R. L. Taylor, and T. L. Brekke, "A model for the mechanics of jointed rock," *Journal of Soil Mechanics and Foundations Division*, vol. 94, no. 3, pp. 637–659, 1968.

[18] J. Yu, G. Y. Liu, Y. Y. Cai, J. F. Zhou, S. Y. Liu, and B. X. Tu, "Time-dependent deformation mechanism for swelling soft-rock tunnels in coal mines and its mathematical deduction," *International Journal of Geomechanics*, vol. 20, no. 3, article 04019186, 2020.

[19] E. J. Garboczi, G. S. Cheok, and W. C. Stone, "Using LADAR to characterize the 3-D shape of aggregates: preliminary results," *Cement and Concrete Research*, vol. 36, no. 6, pp. 1072–1075, 2006.

[20] S. Häfner, S. Eckardt, T. Luther, and C. Konke, "Mesoscale modeling of concrete: geometry and numerics," *Computers and Structures*, vol. 84, no. 7, pp. 450–461, 2006.

[21] Z. M. Wang, A. K. H. Kwan, and H. C. Chan, "Mesoscopic study of concrete I: generation of random aggregate structure and finite element mesh," *Computers and Structures*, vol. 70, no. 5, pp. 533–544, 1999.

[22] H. Z. Cui, T. Y. Lo, S. A. Memon, and W. T. Xu, "Effect of lightweight aggregates on the mechanical properties and brittleness of lightweight aggregate concrete," *Construction and Building Materials*, vol. 35, no. 10, pp. 149–158, 2012.

[23] H. Kim and W. G. Buttlar, "Discrete fracture modeling of asphalt concrete," *International Journal of Solids and Structures*, vol. 46, no. 13, pp. 2593–2604, 2009.

[24] K. R. Wu, B. Chen, W. Yao, and D. Zhang, "Effect of coarse aggregate type on mechanical properties of high-performance concrete," *Cement and Concrete Research*, vol. 31, no. 10, pp. 1421–1425, 2001.

[25] L. P. Li, J. Hu, S. C. Li et al., "Development of a novel triaxial rock testing method based on biaxial test apparatus and its application," *Rock Mechanics and Rock Engineering*, vol. 54, no. 3, pp. 1597–1607, 2021.

[26] M. Bourke, H. Viles, J. Nicoli, P. Lyew-Ayee, R. Ghent, and J. Holmlund, "Innovative applications of laser scanning and rapid prototype printing to rock breakdown experiments," *Earth Surface Processes and Landforms*, vol. 33, no. 10, pp. 1614–1621, 2008.

[27] W. Otten, R. Pajor, S. Schmidt, P. C. Baveye, R. Hague, and R. E. Falconer, "Combining X-ray CT and 3D printing technology to produce microcosms with replicable, complex pore geometries," *Soil Biology and Biochemistry*, vol. 51, pp. 53–55, 2012.

[28] D. P. Germann, W. Schatz, and P. Eggenberger Hotz, "Artificially evolved functional shell morphology of burrowing bivalves," *Palaeontologia Electronica*, vol. 17, no. 1, pp. 1–25, 2014.

[29] X. W. Feng, F. Xue, T. Z. Wang, L. X. Wang, T. Y. Zhao, and X. X. Liu, "Reinforcing effects of 3D printed bolts on joint-separated standard soft rock specimens," *Composites Part B: Engineering*, vol. 193, article 108024, 2020.

[30] Y. Ju, H. P. Xie, Z. M. Zheng et al., "Visualization of the complex structure and stress field inside rock by means of 3D printing technology," *Science Bulletin*, vol. 59, no. 36, pp. 5354–5365, 2014.

[31] Y. Ju, L. Wang, H. P. Xie, G. W. Ma, Z. M. Zheng, and L. T. Mao, "Visualization and transparentization of the structure and stress field of aggregated geomaterials through 3D printing and photoelastic techniques," *Rock Mechanics and Rock Engineering*, vol. 50, no. 6, pp. 1383–1407, 2017.

[32] Y. Ju, L. Wang, H. Xie et al., "Visualization of the three-dimensional structure and stress field of aggregated concrete materials through 3D printing and frozen-stress techniques," *Construction and Building Materials*, vol. 143, no. 7, pp. 121–137, 2017.

[33] P. Liu, Y. Ju, P. G. Ranjith, Z. M. Zheng, L. Wang, and A. Wanniarachchi, "Visual representation and characterization of three-dimensional hydrofracturing cracks within heterogeneous rock through 3D printing and transparent models," *International Journal of Coal Science and Technology*, vol. 3, no. 3, pp. 284–294, 2016.

[34] J. Jaber, M. Conin, O. Deck, M. Moumni, O. Godard, and S. Kenzari, "Investigation of the mechanical behavior of 3D printed polyamide-12 joints for reduced scale models of rock mass," *Rock Mechanics and Rock Engineering*, vol. 53, no. 6, pp. 2687–2705, 2020.

[35] B. Primkulov, J. Chalaturnyk, R. Chalaturnyk, and G. Zambrano Narvaez, "3D printed sandstone strength: curing of furfuryl alcohol resin-based sandstones," *3D Printing and Additive Manufacturing*, vol. 4, no. 3, pp. 149–156, 2017.

[36] J. S. Gomez, R. J. Chalaturnyk, and G. Zambrano-Narvaez, "Experimental investigation of the mechanical behavior and permeability of 3D printed sandstone analogues under triaxial conditions," *Transport in Porous Media*, vol. 129, no. 2, pp. 541–557, 2019.

[37] C. Jiang and G. F. Zhao, "A preliminary study of 3D printing on rock mechanics," *Rock Mechanics and Rock Engineering*, vol. 48, no. 3, pp. 1041–1050, 2015.

[38] C. Jiang, G. F. Zhao, J. B. Zhu, Y. X. Zhao, and L. M. Shen, "Investigation of dynamic crack coalescence using a gypsum-like 3D printing material," *Rock Mechanics and Rock Engineering*, vol. 49, no. 10, pp. 3983–3998, 2016.

[39] Q. Jiang, X. T. Feng, Y. H. Gong, L. B. Song, S. G. Ran, and J. Cui, "Reverse modelling of natural rock joints using 3D scanning and 3D printing," *Computers and Geotechnics*, vol. 73, no. 3, pp. 210–220, 2016.

[40] Q. Jiang, X. T. Feng, L. B. Song, Y. H. Gong, H. Zheng, and J. Cui, "Modeling rock specimens through 3D printing: tentative experiments and prospects," *Acta Mechanica Sinica*, vol. 32, no. 1, pp. 101–111, 2016.

[41] D. Head and T. Vanorio, "Effects of changes in rock microstructures on permeability: 3-D printing investigation," *Geophysical Research Letters*, vol. 43, no. 14, pp. 7494–7502, 2016.

[42] Y. J. Xia, C. Q. Zhang, H. Zhou et al., "Structural characteristics of columnar jointed basalt in drainage tunnel of Baihetan hydropower station and its influence on the behavior of P-wave anisotropy," *Engineering Geology*, vol. 264, article 105304, 2020.

[43] Y. J. Xia, C. Q. Zhang, H. Zhou et al., "Mechanical behavior of structurally reconstructed irregular columnar jointed rock mass using 3D printing," *Engineering Geology*, vol. 268, article 105509, 17 pages, 2020.

[44] Y. J. Xia, C. Q. Zhang, H. Zhou et al., "Study on model structure and mechanical anisotropy of columnar jointed rock mass based on three-dimensional printing method," *International Journal of Geomechanics*, vol. 20, no. 11, article 04020208, 2020.

[45] E. M. Gell, S. M. Walley, and C. H. Braithwaite, "Review of the validity of the use of artificial specimens for characterizing the mechanical properties of rocks," *Rock Mechanics and Rock Engineering*, vol. 52, no. 9, pp. 2949–2961, 2019.

[46] D. Espalin, D. W. Muse, E. Macdonald, and R. B. Wicker, "3D printing multifunctionality: structures with electronics," *International Journal of Advanced Manufacturing Technology*, vol. 72, no. 5-8, pp. 963–978, 2014.

[47] S. R. Rajpurohit and H. K. Dave, "Flexural strength of fused filament fabricated (FFF) PLA parts on an open-source 3D printer," *Advances in Manufacturing*, vol. 6, no. 4, pp. 430–441, 2018.

[48] V. C. F. Li, C. K. Dunn, Z. Zhang, Y. L. Deng, and H. J. Qi, "Direct ink write (DIW) 3D printed cellulose nanocrystal aerogel structures," *Scientific Reports*, vol. 7, no. 1, pp. 1–8, 2017.

[49] M. Spoerk, C. Savandaiah, F. Arbeiter et al., "Anisotropic properties of oriented short carbon fibre filled polypropylene parts fabricated by extrusion-based additive manufacturing," *Composites Part A: Applied Science and Manufacturing*, vol. 113, no. 1, pp. 95–104, 2018.

[50] X. Feng, F. Xue, T. Wang, L. Wang, T. Zhao, and X. Liu, "3D printing a mechanically-tunable acrylate resin on a cmmercial DLP-SLA printer," *Additive Manufacturing*, vol. 1, no. 23, pp. 374–380, 2018.

[51] C. J. Bloomquist, M. B. Mecham, M. D. Paradzinsky et al., "Controlling release from 3D printed medical devices using CLIP and drug-loaded liquid resins," *Journal of Controlled Release*, vol. 278, no. 28, pp. 9–23, 2018.

[52] H. S. Shang and Y. P. Song, "Triaxial compressive strength of air-entrained concrete after freeze-thaw cycles," *Cold Regions Science and Technology*, vol. 90-91, no. 91, pp. 33–37, 2013.

[53] A. T. Sidambe, I. Todd, and P. V. Hatton, "Effects of build orientation induced surface modifications on thein vitrobiocompatibility of electron beam melted Ti6Al4V," *Powder Metallurgy*, vol. 59, no. 1, pp. 57–65, 2016.

[54] C. L. Wang and S. W. Qi, "Application and prospect of 3D printing for rock mechanics," *Progress in Geophysics*, vol. 33, no. 2, pp. 842–849, 2018, (in Chinese).

[55] Q. B. Nguyen, D. N. Luu, S. M. L. Nai, Z. Zhu, Z. Chen, and J. Wei, "The role of powder layer thickness on the quality of SLM printed parts," *Archives of Civil and Mechanical Engineering*, vol. 18, no. 3, pp. 948–955, 2018.

[56] F. Fina, A. Goyanes, C. M. Madla et al., "3D printing of drug-loaded gyroid lattices using selective laser sintering," *International Journal of Pharmaceutics*, vol. 547, no. 1-2, pp. 44–52, 2018.

[57] M. A. al-Tarifi and D. S. Filipovic, "On the design and fabrication of W-band stabilised-pattern dual-polarised horn antennas with DMLS and CNC," *IET Microwaves, Antennas & Propagation*, vol. 11, no. 14, pp. 1930–1935, 2017.

[58] W. Gao, Y. B. Zhang, D. Ramanujan et al., "The status, challenges, and future of additive manufacturing in engineering," *Computer-Aided Design*, vol. 69, pp. 65–89, 2015.

[59] H. Jee and M. Kim, "Spherically curved layer (SCL) model for metal 3-D printing of overhangs," *Journal of Mechanical Science and Technology*, vol. 31, no. 12, pp. 5729–5735, 2017.

[60] Y. Ju, Z. Y. Ren, X. L. Li, Y. T. Wang, L. T. Mao, and F. P. Chiang, "Quantification of hidden whole-field stress inside porous geomaterials via three-dimensional printing and photoelastic testing methods," *Journal of Geophysical Research Solid Earth*, vol. 124, no. 6, pp. 5408–5426, 2019.

[61] Y. Ju, Z. Zheng, H. Xie, J. Lu, L. Wang, and K. He, "Experimental visualisation methods for three-dimensional stress fields of porous solids," *Experimental Techniques*, vol. 41, no. 4, pp. 331–344, 2017.

[62] Y. Ju, C. B. Wan, Z. Y. Ren, L. T. Mao, G. Fu, and F. P. Chiang, "Quantification of continuous evolution of full-field stress associated with shear deformation of faults using three-dimensional printing and phase- shifting methods," *International Journal of Rock Mechanics and Mining Sciences*, vol. 126, article 104187, 2020.

[63] Y. Ju, Z. Y. Ren, J. T. Zheng et al., "Quantitative visualization methods for continuous evolution of three- dimensional discontinuous structures and stress field in subsurface rock mass induced by excavation and construction - an overview," *Engineering Geology*, vol. 265, article 105443, 2020.

[64] K. R. Hart and E. D. Wetzel, "Fracture behavior of additively manufactured acrylonitrile butadiene styrene (ABS) materials," *Engineering Fracture Mechanics*, vol. 177, pp. 1–13, 2017.

[65] S. Fereshtenejad and J. J. Song, "Fundamental study on applicability of powder-based 3D printer for physical modeling in rock mechanics," *Rock Mechanics and Rock Engineering*, vol. 49, no. 6, pp. 2065–2074, 2016.

[66] M. A. Perras and D. Vogler, "Compressive and tensile behavior of 3D-printed and natural sandstones," *Transport in Porous Media*, vol. 129, no. 2, pp. 559–581, 2019.

[67] T. Zhou and J. B. Zhu, "Identification of a suitable 3D printing material for mimicking brittle and hard rocks and its brittleness enhancements," *Rock Mechanics and Rock Engineering*, vol. 51, no. 3, pp. 765–777, 2018.

[68] C. R. Deckard, *Method and apparatus for producing parts by selective sintering*, no. article 5017753, 1989DC: US Patent Office, 1989.

[69] X. L. Li, J. X. Ma, P. Li, Q. Chen, and W. M. Zhou, "3D printing technology and its application trend," *Process Automation Instrumentation*, vol. 35, no. 1, pp. 1–5, 2014.

[70] Z. L. Li, L. Li, C. Wang, and G. Liu, "The 3D printing technology and the application research in petrochemical industry," *Guangdong Chemical Industry*, vol. 41, no. 23, pp. 100-101, 2014.

[71] K. J. Hodder and J. A. Nychka, "Silane treatment of 3D-printed sandstone models for improved spontaneous imbibition of water," *Transport in Porous Media*, vol. 129, no. 2, pp. 583–598, 2019.

[72] K. Barbosa, R. Chalaturnyk, B. Bonfils, J. Esterle, and Z. W. Chen, "Testing impact load cell calculations of material fracture toughness and strength using 3D-printed sandstone," *Geotechnical and Geological Engineering*, vol. 38, no. 2, pp. 1065–1096, 2020.

[73] Z. J. Wu, B. Zhang, L. Weng, Q. S. Liu, and L. N. Y. Wong, "A new way to replicate the highly stressed soft rock: 3D printing exploration," *Rock Mechanics and Rock Engineering*, vol. 53, no. 1, pp. 467–476, 2020.

[74] L. B. Song, Q. Jiang, Y. E. Shi et al., "Feasibility investigation of 3D printing technology for geotechnical physical models: study of tunnels," *Rock Mechanics and Rock Engineering*, vol. 51, no. 8, pp. 2617–2637, 2018.

[75] L. Y. Kong, M. Ostadhassan, B. Liu, C. X. Li, and K. Q. Liu, "Multifractal characteristics of MIP-based pore size distribution of 3D-printed powder-based rocks: a study of post-processing effect," *Transport in Porous Media*, vol. 129, no. 2, pp. 599–618, 2019.

[76] L. Y. Kong, M. Ostadhassan, S. Zamiran, B. Liu, C. X. Li, and G. G. Marino, "Geomechanical upscaling methods: comparison and verification via 3D printing," *Energies*, vol. 12, no. 3, article 382, 2019.

[77] M. H. Shen, W. Qin, B. H. Xing et al., "Mechanical properties of 3D printed ceramic cellular materials with triply periodic minimal surface architectures," *Journal of the European Ceramic Society*, vol. 41, no. 2, pp. 1481–1489, 2021.

[78] X. T. Feng, Y. H. Gong, Y. Y. Zhou, Z. W. Li, and X. F. Liu, "The 3D-printing technology of geological models using rock-like materials," *Rock Mechanics and Rock Engineering*, vol. 52, no. 7, pp. 2261–2277, 2019.

[79] G. W. Ma, Z. J. Li, L. Wang, F. Wang, and J. Sanjayan, "Mechanical anisotropy of aligned fiber reinforced composite for extrusion- based 3D printing," *Construction and Building Materials*, vol. 202, pp. 770–783, 2019.

[80] R. Song, Y. Wang, S. Ishutov et al., "A comprehensive experimental study on mechanical behavior, microstructure and transport properties of 3D-printed rock analogs," *Rock Mechanics and Rock Engineering*, vol. 53, no. 12, pp. 5745–5765, 2020.

[81] K. J. Hodder, J. A. Nychka, and R. J. Chalaturnyk, "Process limitations of 3D printing model rock," *Progress in Additive Manufacturing*, vol. 3, no. 3, pp. 173–182, 2018.

[82] M. Sharafisafa, L. M. Shen, Y. G. Zheng, and J. Z. Xiao, "The effect of flaw filling material on the compressive behaviour of 3D printed rock-like discs," *International Journal of Rock Mechanics and Mining Sciences*, vol. 117, pp. 105–117, 2019.

[83] M. Sharafisafa and L. M. Shen, "Experimental investigation of dynamic fracture patterns of 3D printed rock-like material under impact with digital image correlation," *Rock Mechanics and Rock Engineering*, vol. 53, no. 8, pp. 3589–3607, 2020.

[84] M. Sharafisafa, Z. Aliabadian, F. Tahmasebinia, and L. M. Shen, "A comparative study on the crack development in rock-like specimens containing unfilled and filled flaws," *Engineering Fracture Mechanics*, vol. 241, article 107405, 2021.

[85] Z. Aliabadian, M. Sharafisafa, F. Tahmasebinia, and L. M. Shen, "Experimental and numerical investigations on crack development in 3D printed rock-like specimens with pre-existing flaws," *Engineering Fracture Mechanics*, vol. 241, article 107396, 2020.

[86] T. Zhou, J. B. Zhu, and H. P. Xie, "Mechanical and volumetric fracturing behaviour of three-dimensional printing rock-like samples under dynamic loading," *Rock Mechanics and Rock Engineering*, vol. 53, no. 6, pp. 2855–2864, 2020.

[87] T. Zhou, J. B. Zhu, Y. Ju, and H. P. Xie, "Volumetric fracturing behavior of 3D printed artificial rocks containing single and double 3D internal flaws under static uniaxial compression," *Engineering Fracture Mechanics*, vol. 205, pp. 190–204, 2019.

[88] L. F. Zhang, F. J. Zhou, J. Y. Mou et al., "Large-scale true triaxial fracturing experimental investigation on diversion behavior of fiber using 3D printing model of rock formation," *Journal of Petroleum Science and Engineering*, vol. 181, article 106171, 2019.

[89] L. R. Ban, C. Z. Qi, H. X. Chen, F. Y. Yan, and C. M. Ji, "A new criterion for peak shear strength of rock joints with a 3D roughness parameter," *Rock Mechanics and Rock Engineering*, vol. 53, no. 4, pp. 1755–1775, 2020.

[90] T. Ishibashi, Y. Fang, D. Elsworth, N. Watanabe, and H. Asanuma, "Hydromechanical properties of 3D printed fractures with controlled surface roughness: insights into shear-permeability coupling processes," *International Journal of Rock Mechanics and Mining Sciences*, vol. 128, article 104271, 2020.

[91] Q. Jiang, L. B. Song, F. Yan, C. Liu, B. Yang, and J. Xiong, "Experimental investigation of anisotropic wear damage for natural joints under direct shearing test," *International Journal of Geomechanics*, vol. 20, no. 4, article 04020015, 2020.

[92] A. Suzuki, N. Watanabe, K. W. Li, and R. N. Horne, "Fracture network created by 3-D printer and its validation using CT images," *Water Resources Research*, vol. 53, no. 7, pp. 6330–6339, 2017.

[93] A. Suzuki, J. M. Minto, N. Watanabe, K. Li, and R. N. Horne, "Contributions of 3D printed fracture networks to development of flow and transport models," *Transport in Porous Media*, vol. 129, no. 2, pp. 485–500, 2019.

[94] D. Bachmann, S. Bouissou, and A. Chemenda, "Influence of weathering and pre-existing large scale fractures on gravitational slope failure: insights from 3-D physical modelling," *Natural hazards and earth system sciences*, vol. 4, no. 5/6, pp. 711–717, 2004.

[95] M. C. He, W. L. Gong, H. M. Zhai, and H. P. Zhang, "Physical modeling of deep ground excavation in geologically horizontal strata based on infrared thermography," *Tunnelling and Underground Space Technology*, vol. 25, no. 4, pp. 366–376, 2010.

[96] Q. Y. Zhang, K. Duan, Y. Y. Jiao, and W. Xiang, "Physical model test and numerical simulation for the stability analysis of deep gas storage cavern group located in bedded rock salt formation," *International Journal of Rock Mechanics and Mining Sciences*, vol. 94, pp. 43–54, 2017.

[97] S. Suwansawat and H. H. Einstein, "Describing settlement troughs over twin tunnels using a superposition technique," *Journal of Geotechnical and Geoenvironmental Engineering*, vol. 133, no. 4, pp. 445–468, 2007.

[98] D. Merlini, D. Stocker, M. Falanesca, and R. Schuerch, "The Ceneri Base Tunnel: construction experience with the southern portion of the flat railway line crossing the Swiss Alps," *Engineering*, vol. 4, no. 2, pp. 235–248, 2018.

[99] M. Afifipour, M. Sharifzadeh, K. Shahriar, and H. Jamshidi, "Interaction of twin tunnels and shallow foundation at Zand underpass, Shiraz metro, Iran," *Tunnelling and Underground Space Technology*, vol. 26, no. 2, pp. 356–363, 2011.

[100] M. Sharifzadeh, A. Tarifard, and M. A. Moridi, "Time-dependent behavior of tunnel lining in weak rock mass based on displacement back analysis method," *Tunnelling and Underground Space Technology*, vol. 38, pp. 348–356, 2013.

[101] M. Tezuka and T. Seoka, "Latest technology of underground rock cavern excavation in Japan," *Tunnelling and Underground Space Technology*, vol. 18, no. 2-3, pp. 127–144, 2003.

[102] N. Plasencia, J. M. Carvalho, and T. Cavaco, "Groundwater monitoring impacts of deep excavations: hydrogeology in the Venda Nova repowering schemes (NW Portugal)," *Environmental Earth Sciences*, vol. 73, no. 6, pp. 2981–2995, 2015.

[103] M. R. Islam and R. Shinjo, "Mining-induced fault reactivation associated with the main conveyor belt roadway and safety of the Barapukuria Coal Mine in Bangladesh: constraints from BEM simulations," *International Journal of Coal Geology*, vol. 79, no. 4, pp. 115–130, 2009.

[104] X. Huang, Q. Liu, K. Shi, Y. C. Pan, and J. P. Liu, "Application and prospect of hard rock TBM for deep roadway construction in coal mines," *Tunnelling and Underground Space Technology*, vol. 73, pp. 105–126, 2018.

[105] Q. Jiang, X. P. Liu, F. Yan, Y. Yang, D. P. Xu, and G. L. Feng, "Failure performance of 3DP physical twin-tunnel model and corresponding safety factor evaluation," *Rock Mechanics and Rock Engineering*, vol. 54, no. 1, pp. 109–128, 2021.

[106] S. Jeon, J. Kim, Y. Seo, and C. Hong, "Effect of a fault and weak plane on the stability of a tunnel in rock–a scaled model test and numerical analysis," *International Journal of Rock Mechanics and Mining Sciences*, vol. 41, no. 3, pp. 486–486, 2004.

[107] D. Sterpi and A. Cividini, "A physical and numerical investigation on the stability of shallow tunnels in strain softening media," *Rock Mechanics and Rock Engineering*, vol. 37, no. 4, pp. 277–298, 2004.

[108] S. Seki, S. Kaise, Y. Morisaki, S. Azetaka, and Y. J. Jiang, "Model experiments for examining heaving phenomenon in tunnels," *Tunnelling and Underground Space Technology*, vol. 23, no. 2, pp. 128–138, 2008.

[109] J. C. Jaeger, "Friction of rocks and stability of rock slopes," *Géotechnique*, vol. 21, no. 2, pp. 97–134, 1971.

[110] P. H. S. W. Kulatilake, G. Shou, T. H. Huang, and R. M. Morgan, "New peak shear strength criteria for anisotropic rock joints," *International Journal of Rock Mechanics and Mining Sciences and Geomechanics Abstracts*, vol. 32, no. 7, pp. 673–697, 1995.

[111] F. Homand, T. Belem, and M. Souley, "Friction and degradation of rock joint surfaces under shear loads," *International Journal for Numerical and Analytical Methods in Geomechanics*, vol. 25, no. 10, pp. 973–999, 2001.

[112] G. C. Zhang, M. Karakus, H. M. Tang, Y. F. Ge, and L. Zhang, "A new method estimating the 2D joint roughness coefficient for discontinuity surfaces in rock masses," *International Journal of Rock Mechanics and Mining Sciences*, vol. 72, pp. 191–198, 2014.

[113] C. Q. Zhang, G. J. Cui, X. R. Chen, H. Zhou, and L. Deng, "Effects of bolt profile and grout mixture on shearing behaviors of bolt-grout interface," *Journal of Rock Mechanics and Geotechnical Engineering*, vol. 12, no. 2, pp. 242–255, 2020.

[114] L. P. Liu, J. Xiao, and Y. Wang, "Major orientation estimation-based rock surface extraction for 3D rock-mass point clouds," *Remote Sensing*, vol. 11, no. 6, article 635, 2019.

[115] A. J. Riquelme, A. Abellán, R. Tomás, and M. Jaboyedoff, "A new approach for semi-automatic rock mass joints recognition from 3D point clouds," *Computers and Geosciences*, vol. 68, pp. 38–52, 2014.

[116] A. J. Riquelme, A. Abellán, and R. Tomás, "Discontinuity spacing analysis in rock masses using 3D point clouds," *Engineering Geology*, vol. 195, pp. 185–195, 2015.

[117] P. T. Wang, T. H. Yang, Q. L. Yu, H. L. Liu, and P. H. Zhang, "Characterization on jointed rock masses based on PFC2D," *Frontiers of Structural and Civil Engineering*, vol. 7, no. 1, pp. 32–38, 2013.

[118] J. Q. Chen, H. H. Zhu, and X. J. Li, "Automatic extraction of discontinuity orientation from rock mass surface 3D point cloud," *Computers and Geosciences*, vol. 95, pp. 18–31, 2016.

[119] Y. F. Ge, Z. G. Xie, H. M. Tang, H. Z. Chen, Z. S. Lin, and B. du, "Determination of shear failure regions of rock joints based on point clouds and image segmentation," *Engineering Geology*, vol. 260, article 105250, 2019.

[120] B. C. Yang, L. Xue, and K. Zhang, "X-ray micro-computed tomography study of the propagation of cracks in shale during uniaxial compression," *Environmental Earth Sciences*, vol. 77, no. 18, article 652, 2018.

[121] S. Q. Yang, P. F. Yin, and Y. H. Huang, "Experiment and discrete element modelling on strength, deformation and failure behaviour of shale under Brazilian compression," *Rock Mechanics and Rock Engineering*, vol. 52, no. 11, pp. 4339–4359, 2019.

[122] Y. T. Duan, X. Li, B. Zheng, J. M. He, and J. Hao, "Cracking evolution and failure characteristics of Longmaxi shale under uniaxial compression using real-time computed tomography scanning," *Rock Mechanics and Rock Engineerin*, vol. 52, no. 9, pp. 3003–3015, 2019.

[123] G. W. Ma, Q. Q. Dong, L. F. Fan, and J. W. Gao, "An investigation of non-straight fissures cracking under uniaxial compression," *Engineering Fracture Mechanics*, vol. 191, pp. 300–310, 2018.

[124] G. W. Ma, Q. Q. Dong, and L. Wang, "Experimental investigation on the cracking behavior of 3D printed kinked fissure," *Science China Earth Sciences*, vol. 61, no. 12, pp. 1872–1881, 2018.

[125] W. Yang, D. Zhang, and G. Lei, "Experimental study on multiphase flow in fracture-vug medium using 3D printing technology and visualization techniques," *Journal of Petroleum Science and Engineering*, vol. 193, article 107394, 2020.

[126] C. Jiang and G. F. Zhao, "Implementation of a coupled plastic damage distinct lattice spring model for dynamic crack propagation in geomaterials," *International Jounal for Numerical and Analytical Methods in Geomechanics*, vol. 42, no. 4, pp. 674–693, 2017.

[127] M. A. Schroedl, J. J. Mcgowan, and C. W. Smith, "An assessment of factors influencing data obtained by the photoelastic stress freezing technique for stress fields near crack tips," *Engineering Fracture Mechanics*, vol. 4, no. 4, pp. 801–809, 1972.

[128] J. S. Epstein, D. Post, and C. W. Smith, "Three-dimensional photoelastic measurements with very thin slices," *Experimental Techniques*, vol. 8, no. 12, pp. 34–37, 1984.

[129] C. Pappalettre and U. Galietti, "Polycarbonate for frozen stress photoelasticity," *Strain*, vol. 31, no. 2, pp. 69–74, 1995.

[130] T. H. Hyde and N. A. Warrior, "An improved method for the determination of photoelastic stress intensity factors using the westergaard stress function," *International Journal of Mechanical Sciences*, vol. 32, no. 3, pp. 265–273, 1990.

[131] C. Buckberry and D. Towers, "New approaches to the full-field analysis of photoelastic stress patterns," *Optics and Lasers in Engineering*, vol. 24, no. 5-6, pp. 415–428, 1996.

[132] A. Baldi, F. Bertolino, and F. Ginesu, "A temporal phase unwrapping algorithm for photoelastic stress analysis," *Optics and Lasers in Engineering*, vol. 45, no. 5, pp. 612–617, 2007.

[133] P. Pinit and E. Umezaki, "Digitally whole-field analysis of isoclinic parameter in photoelasticity by four-step color phase-shifting technique," *Optics and Lasers in Engineering*, vol. 45, no. 7, pp. 795–807, 2007.

[134] J. P. Kruth, M. C. Leu, and T. Nakagawa, "Progress in additive manufacturing and rapid prototyping," *CIRP Annals*, vol. 47, no. 2, pp. 525–540, 1998.

[135] H. J. Jee and E. Sachs, "A visual simulation technique for 3D printing," *Advances in Engineering Software*, vol. 31, no. 2, pp. 97–106, 2000.

[136] B. W. Miller, J. W. Moore, H. H. Barrett et al., "3D printing in X-ray and gamma-ray imaging: a novel method for fabricating high-density imaging apertures," *Nuclear Instruments and Methods in Physics Research Section A: Accelerators, Spectrometers, Detectors and Associated Equipment*, vol. 659, no. 1, pp. 262–268, 2011.

[137] T. A. Campbell and O. S. Ivanova, "3D printing of multifunctional nanocomposites," *Nano Today*, vol. 8, no. 2, pp. 119-120, 2013.

[138] V. Kostakis and M. Papachristou, "Commons-based peer production and digital fabrication: the case of a RepRap-based, Lego-built 3D printing-milling machine," *Telematics and Informatics*, vol. 31, no. 3, pp. 434–443, 2014.

[139] M. Salcher and R. Bertuzzi, "Results of pull tests of rock bolts and cable bolts in Sydney sandstone and shale," *Tunnelling and Underground Space Technology*, vol. 74, pp. 60–70, 2018.

[140] A. H. Hoien, B. Nilsen, and R. Olsson, "Main aspects of deformation and rock support in Norwegian road tunnels," *Tunnelling and Underground Space Technology*, vol. 86, pp. 262–278, 2019.

[141] G. Desbois, J. Urai, and P. Kukla, "Morphology of the pore space in claystones – evidence from BIB/FIB ion beam sectioning and cryo-SEM observations," *eEarth Discuss*, vol. 4, no. 1, pp. 1–19, 2009.

[142] S. Hemes, G. Desbois, J. L. Urai, M. De Craen, and M. Honty, "Variations in the morphology of porosity in the Boom Clay Formation: insights from 2D high resolution BIB-SEM imaging and mercury injection porosimetry," *Netherlands Journal of Geosciences*, vol. 92, no. 4, pp. 275–300, 2013.

[143] R. Yang, S. He, J. Z. Yi, and Q. H. Hu, "Nano-scale pore structure and fractal dimension of organic-rich Wufeng- Longmaxi shale from Jiaoshiba area, Sichuan Basin: investigations using FE- SEM, gas adsorption and helium pycnometry," *Marine and Petroleum Geology*, vol. 70, pp. 27–45, 2016.

[144] M. E. Houben, G. Desbois, and J. L. Urai, "A comparative study of representative 2D microstructures in shaly and sandy facies of opalinus clay (Mont Terri, Switzerland) inferred form BIB-SEM and MIP methods," *Marine and Petroleum Geology*, vol. 49, pp. 143–161, 2014.

[145] M. E. Houben, G. Desbois, and J. L. Urai, "Pore morphology and distribution in the Shaly facies of Opalinus Clay (Mont Terri, Switzerland): insights from representative 2D BIB-SEM investigations on mm to nm scale," *Applied Clay Science*, vol. 71, pp. 82–97, 2013.

[146] K. Jiao, S. P. Yao, C. Liu et al., "The characterization and quantitative analysis of nanopores in unconventional gas reservoirs utilizing FESEM-FIB and image processing: an example from the lower Silurian Longmaxi Shale, upper Yangtze region, China," *International Journal of Coal Geology*, vol. 128-129, pp. 1–11, 2014.

[147] J. Klaver, G. Desbois, R. Littke, and J. L. Urai, "BIB-SEM characterization of pore space morphology and distribution in postmature to overmature samples from the Haynesville and Bossier Shales," *Marine and Petroleum Geology*, vol. 59, pp. 451–466, 2015.

[148] J. Klaver, G. Desbois, J. L. Urai, and R. Littke, "BIB-SEM study of the pore space morphology in early mature Posidonia Shale from the Hils area, Germany," *International Journal of Coal Geology*, vol. 103, no. 1, pp. 12–25, 2012.

[149] Y. Wang, Y. F. Yi, C. H. Li, and J. Q. Han, "Anisotropic fracture and energy characteristics of a Tibet marble exposed to multi-level constant-amplitude (MLCA) cyclic loads: a lab-scale testing," *Engineering Fracture Mechanics*, vol. 244, article 107550, 2021.

[150] Y. Wang, B. Zhang, B. Li, and C. H. Li, "A strain-based fatigue damage model for naturally fractured marble subjected to freeze-thaw and uniaxial cyclic loads," *International Journal of Damage Mechanics*, 2021.

[151] Y. Wang, C. H. Li, and J. Q. Han, "On the effect of stress amplitude on fracture and energy evolution of pre- flawed granite under uniaxial increasing-amplitude fatigue loads," *Engineering Fracture Mechanics*, vol. 240, article 107366, 17 pages, 2020.

[152] Y. Wang, W. K. Feng, H. J. Wang, C. H. Li, and Z. Q. Hou, "Rock bridge fracturing characteristics in granite induced by freeze-thaw and uniaxial deformation revealed by AE monitoring and post-test CT scanning," *1036 Cold Regions Science and Technology*, vol. 177, article 103115, 2020.

[153] Y. Wang, C. H. Li, J. Hao, and R. Q. Zhou, "X-ray microtomography for investigation of meso-structural changes and crack evolution in Longmaxi formation shale during compressive deformation," *Journal of Petroleum Science and Engineering*, vol. 164, pp. 278–288, 2018.